Life-history variation mediates the importance of population structure to the short-term dynamics of plant populations worldwide

James Cant[1,*], Christina M. Hernández[1], David N. Koons[2], Dave J. Hodgson[3], Man Qi[1], Andrew Hector[1], Iain Stott[4], Roberto Salguero-Gómez[1,*]

1. Department of Biology, University of Oxford, Oxford, UK.
2. Department of Fish, Wildlife, and Conservation Biology, Colorado State University, USA.
3. Department of Ecology & Evolution, University of Exeter, UK.
4. Department of Life Sciences, University of Lincoln, Lincoln, UK.

*Corresponding Authors: **Email:** james.cant91@gmail.com; rob.salguero@biology.ox.ac.uk

Author Contributions: RS-G devised the initial research idea with further input from DK. This idea was then further developed by JC, CH & RS-G. JC & CH identified and extracted population models for the analyses from a database curated by RS-G, while RS-G, DH & JC contributed population vectors. JC implemented all the analyses, shaped by discussions between JC, CH, MQ & RS-G. RS-G led efforts to secure research funding, with IS and AH contributing as CoIs. JC led manuscript write-up with support from RS-G, with all coauthors contributing equally to the development of subsequent drafts.

Competing Interest Statement: All authors declare no competing interests.

Keywords: Plants, Resilience, Structured Population Models, Transient Life Table Response Experiment.

Abstract

A population's structure (*i.e.*, the distribution of individuals across the life cycle of a species) influences how it responds to environmental changes and recurrent disturbances, and shapes its vulnerability to extinction. Yet, despite compelling evidence that population structures are rarely stationary over time, assessments of population viability have only recently begun to consider how a population's structure interacts with its vital rates of survival, development, and fecundity to determine its demographic performance. Using 268 comparisons of population dynamics in 56 plant species across differing time periods, locations, and/or experimental treatments, we use transient Life Table Response Experiments (tLTREs) to quantify how changes in population structure and vital rates contribute to observed variation in demographic performance. We illustrate how changes in population structure are major contributors to short-term (*i.e.* transient) demographic performance, and are just as important as the effects of, more routinely evaluated, changes in survival and fecundity rates for informing population viability assessments. Moreover, these contribution patterns challenge prevailing understanding of the links between plant growth form and population viability. Accordingly, we emphasise how quantifying the effects of population structure on transient population dynamics can reveal key mechanistic insights necessary for accurately predicting the responses of natural populations worldwide to ongoing global change. Indeed, linking the structure and dynamics of natural populations is essential for the effective management and conservation of global biodiversity.

Significance Statement

Using 268 comparisons of population dynamics in 56 plant species across different time periods, locations, and/or experimental treatments, we show how changes in population structure are just as important as the effects of changing survival and fecundity rates in determining population viability; particularly in shorter-lived species. Current assessments of population viability largely focus on evaluating how changing vital rates affect population dynamics. However, the critical role of population structure in mediating population dynamics evidences how current efforts to forecast plant populations and communities are incomplete. As such, we emphasise the need for explicitly including population structure in assessments of demographic performance and resilience for the effective management of natural populations.

Introduction

Historically, assessments of population viability typically evaluate how individual-level patterns in survival, development, and fecundity respond to disturbances and environmental fluctuations (*e.g.*, seasonal cycles, drought, forest forest etc.) (1). Indeed, transient (*i.e.*, short-term; although some transient cycles can persist over long periods (2)) variation in these vital rates underpins the resistance and recovery potential of natural populations (3). However, demographic performance (*i.e.,* a population's growth rate) arises from an interaction between a population's vital rates and its structure (4). Survival, development, and fecundity rates shape the structure of populations to directly inform their realised performance (5, 6) (Fig. 1A). Unless a population possesses a stable structure, whereby it will change in size at a constant rate over time (its long-term population growth rate, λ), its vital rates will change the age- (7), size- (8), developmental stage- (9), or other state-distribution (*e.g.*, sex ratio (10)) of the individuals within the population. Accordingly, population trajectories comprise the direct and indirect effects of stochastic and disturbance-induced variability across both the vital rates and structure of populations (11, 12). Thus, accounting for population structure, a feature that is rarely done in demography (5, 13), can provide greater mechanistic insight into demographic performance and resilience (14), though to what extent remains unquantified.

Periodic disturbances and/or environmental shifts prevent populations from attaining their stable population structure or stationary growth trajectory (*i.e.*, λ) (15). Instead, populations are maintained within a transient state during which their realised growth rates ($\lambda_{transient}$) change through time and/or space (16). The transient Life Table Response Experiment framework (4) (*tLTRE*, hereafter) was introduced as a way to decompose this variation in $\lambda_{transient}$ into the contributions provided by underlying shifts in observed vital rates and population structure (4, 11)

(Fig. 1B). tLTREs have since been implemented in the case-specific assessment of various mammal (*e.g.*, (5, 6, 17)) and bird species (*e.g.*, (14, 18–21)). However, while theory predicts a link between life-history variation and the contributions of population structure to variation in $\lambda_{transient}$ (4), how population structure influences realised demographic performance across natural populations and life-history strategies remains untested.

Here, to assess how the contribution of population structure to variation in demographic performance corresponds with established axes of life-history variation, we apply tLTREs to 268 comparisons of population dynamics in 56 plant species across differing time periods, locations, and/or experimental treatments (22). Specifically, we test the following hypotheses: (*H1*) Observed variation in population structure will elicit comparable contributions to variance in $\lambda_{transient}$ to those from observed fluctuations in population vital rates. Our rationale for this expectation is that changes to population vital rates do not occur independently of changes to population structure, and instead comprise the indirect effects of changing population structures (4, 11, 23). However, we expect that (*H2*) the relative importance of contributions from population structure will be greater in species with faster life-histories (*e.g.*, shorter generation times (24)). Indeed, the low survival associated with shorter-lived species renders individuals more susceptible to abiotic anomalies, compared to longer-lived species (25), and thus their population structures are likely more variable through time. Concurrently, we predict that (*H3*) greater increases in survival across the life cycle of a population will be associated with increased contributions from variation in population structure to variance in $\lambda_{transient}$. Our rationale here is that low survival early in the life cycle suggests that species invest little into offspring survival (*i.e.*, smaller seed size), a characteristic associated with faster-lived plant species (26).

We also expect that (*H4*) increasing iteroparity will be associated with decreased contributions from variation in population structure to variance in $\lambda_{transient}$. Iteroparous species typically have lengthened reproductive windows and thus likely more opportunities to contribute new individuals to their populations (27). As such, demographic performance in these species is likely less sensitive to changes in the distribution of individuals across their life cycle. However, we anticipate that (*H5*) observed relationships between sources of variance in demographic performance and life-history strategies will be strongly mediated by plant growth form, with contributions from changes in population structure becoming increasingly important in species whose anatomy does not allow for the seasonal loss of aboveground biomass (*e.g.*, American beech, *Fagus grandifolia*) compared to those that do (*e.g.*, Cowslip, *Primula veris*). Plant species whose individuals physically recede during overwintering periods likely experience more frequent changes in their population structure, and so the dynamics of these species should be less sensitive to changes in population structure.

Results

Population structure cannot be overlooked

Fluctuations in population structure have similar impacts on variance in demographic performance as changes in the population vital rates (Fig. 2A). We used tLTREs to test how (*H1*) contributions from changes in population structure ($\boldsymbol{n}$) to observed variance in $\lambda_{transient}$ compared to the contributions from changes in survival (σ), development (γ), and fecundity (ϕ). To do so, we partitioned observed variance in $\lambda_{\text{transient}}$ across our 268 comparisons of plant population dynamics into the contributions from associated changes in population vital rates, structure, and their interactions. Changes in any one of the vital rates or population structure increase observed variance in demographic performance (Fig. 2A). Meanwhile, the effects of the interactions between changes across the vital rates (σ:γ:ϕ) and between the vital rates and population structure (σ:γ:ϕ:$\boldsymbol{n}$) can both dampen or amplify variance observed in demographic performance (Fig. 2A). Selective pressures determine how organisms allocate finite energetic resources between survival and reproduction (28). Accordingly, the impacts of changing survival and fecundity patterns on demographic performance routinely form the crux of assessments into population viability (29, 30) and coexistence theory (31). However, we show that the impact of observed variation in population structure on demographic performance is comparable to that of shifts in survival and fecundity (Fig. 2A); a pattern that is insensitive to data imputations carried out during our analyses (Fig. S9A). Thus, overlooking the effect of a population's structure on its demographic performance can hinder the effective management of natural populations (32).

Like the effects of survival, development, and fecundity, the contribution of population structure to variance in $\lambda_{transient}$ exhibits a strong phylogenetic signal (Fig. 2A). To further evaluate (*H1*) how the effect of population structure on demographic performance compares to the impacts of the vital rates, we tested the strength of phylogenetic signal across our estimates of the contributions of changes in population vital rates and structure to observed variance in $\lambda_{transient}$. We estimated phylogenetic signal using Pagel's Λ (33). We highlight the difference between λ, which represents the long-term growth rate of a population (34), and Pagel's Λ, a proxy of phylogenetic inertia that ranges between 0 and 1. High phylogenetic signal (Pagel's $\Lambda \approx 1$) suggests that the value of a trait of interest is likely more similar in more closely related species (35). As such, patterns in the contribution of population structure to variance in demographic performance appear shaped by species ancestry (Pagel's Λ = 0.65 [95%

CI: 0.37, 0.83]; Fig. 2A). However, this signal is not as strong as that observed across the contributions of survival (σ), development (γ), fecundity (ϕ) and their interactions (σ:γ:ϕ) (Pagel's Λ > 0.80; Fig. 2A). Meanwhile, the contribution of interactions between population structure and vital rates (σ:γ:ϕ:$\boldsymbol{n}$) displays a low phylogenetic signal (Pagel's Λ = 0.25 [0.03, 0.61]), suggesting that the effects of these interactions on short-term demographic performance are shaped by the environment, rather than phylogenetic ancestry.

Contributions of population structure to demographic performance align with the fast-slow continuum

We found support for our hypothesis (*H2*) that the relative contributions of variation in population structure to variance in demographic performance would increase with increasing life-history speed (Fig. 2B). We carried out a phylogenetically informed partial least squares analysis (pPLS) to assess the relationship of our measures of the contributions of changes in survival, development, fecundity, and population structure, with size-scaled measures of generation time (*T*), age at reproductive maturity (L_{α}), mean life expectancy (η_e), and reproductive window ($L_{\alpha\text{-}\omega}$; Table 1) computed from the mean model represented across each population comparison. These four life-history measures form a well-defined trait space that can be used to position species and their populations along two dominant axes of life-history variation: the fast-slow and reproductive strategy continua (27, 36).

Changes in population structure ($\boldsymbol{n}$) typically have the greatest contributions to variance in short-term demographic performance across population comparisons in species with shorter generation times (Fig. 2B). In contrast, the population comparisons of species with longer generation times show greater contributions to variance in demographic performance from changes in survival (σ) and development (γ) (Fig. 2B). Meanwhile, population comparisons exhibiting higher variance in $\lambda_{transient}$ align along an axis associated with the contributions of the interaction between population structure and vital rates (σ:γ:ϕ:$\boldsymbol{n}$) (Fig 2B). Thus, our findings suggest that accommodating population structure is important when assessing demographic performance (Fig. 2A), but that including population structure will not change the key role survival has been demonstrated to play in driving the short-term dynamics of populations with slow life-histories (*e.g.*, Malva nut, *Scaphium borneense* (37)). However, to accurately forecast the demographic performance of short-lived species, we show that quantifying changes in population structure is essential.

We found evidence supporting our hypothesis (*H3*) that species with life cycle survival profiles ($\Delta\sigma$) associated with low offspring survival experience higher contributions from population structure to variance in demographic performance (Fig. 3A). We used phylogenetically informed Bayesian multilevel modelling to test the relationship between measures of contribution ratio (C_{ratio}) and the additive effects of size-scaled measures of mean lifetime survival and life cycle survival profile ($\underline{\sigma}$ & $\Delta\sigma$; Table 1) obtained across our 268 population comparisons. We estimated C_{ratio} as the sum of the main-effect and interaction contributions involving population structure ($\boldsymbol{n}$ & σ:γ:ϕ:$\boldsymbol{n}$) divided by the sum of the main-effect and interaction contributions involving vital rates only (σ, γ, ϕ and σ:γ:ϕ). Thus, contribution ratio provides a measure of the relative contributions from population structure *vs.* vital rates to variance in demographic performance, with $C_{ratio} > 1$ indicating a greater influence of population structure. This observed relationship between $\Delta\sigma$ and C_{ratio}, although consistent across plant growth forms, becomes steeper in species who retain more above-ground biomass during unfavourable growth intervals

(Fig. 3B); represented here by the transition from hemicryptophytes (*i.e.*, plants whose shoot meristems recede to ground level during overwintering periods), to chamaephytes (*i.e.*, woody plants whose shoot meristems remain above ground, but lower than ~ 25 cm, during overwintering periods), and phanerophytes (*i.e.*, woody plants whose shoot meristems remain higher than 25 cm aboveground during overwintering periods; Fig. 3B). We note here, that although represented in our dataset, we do not show the pattern observed for epiphytic plant populations due to them only representing a limited range along our $\Delta\sigma$ scale (Fig. S2).

Modelling the relationship between degree of iteroparity (*S*) and contribution ratio (C_{ratio}; Fig. 4A) offers little support to our hypothesis (*H4*) that the importance of contributions of population structure to demographic performance would decrease with increasing iteroparity. However, including Raunkiær growth form as a fixed effect reveals important heterogeneity across plant types, thus partially supporting *H5*, with C_{ratio} decreasing with increasing iteroparity in both hemicryptophytes (*e.g.* Hoary plantain, *Plantago media*, and Sticklewort, *Agrimonia eupatoria*; Fig. 4B, left) and phanerophytes (*e.g.,* shrubs like Palor palm, *Chamaedorea elegans*, or trees like the Sugar maple, *Acer saccharum;* Fig. 4B, right). Iteroparity affords species increased opportunity for contributing offspring throughout their life cycle, thus reducing their sensitivity to the loss of juvenile life stages (38). Iteroparous species are also better able to take advantage of reproductive strategies maximising reproductive output during periods of favourable conditions (*e.g.*, masting), potentially buffering their demographic performance against increased stochasticity (39). However, that a negative relationship between iteroparity (*S*) and the contribution of population structure to demographic performance is not ubiquitous across plant species emphasizes the importance of evaluating the contextual role population structure plays in influencing population dynamics.

Before interpreting patterns in the relationship between contribution ratio (C_{ratio}) and our measures of life cycle survival profile ($\Delta\sigma$) and degree of iteroparity (S) across plant growth forms, it is necessary to consider the analytical pipeline of a tLTRE. Indeed, contributions to variance in short-term demographic performance derived from tLTREs comprise both the sensitivity of $\lambda_{transient}$ to population parameters as well as the magnitude by which these parameters changed empirically in our dataset (4). Summarising the contribution ratios (C_{ratio}) exhibited across epiphytes (*i.e.*, plants who non-parasitically grow on other plants, like Bird's nest Fern, *Asplenium nidus*), hemicrytophytes, chamaephytes (*e.g.,* Periwinkle, *Vinca minor*), and phanerophytes, it becomes apparent that contributions from population structure are not only more important in species that exhibit seasonal individual-level shrinkage (*e.g.*, hemicryptophytes like *P. veris*), but also in phanerophytes, slow-growing trees and shrubs that invest more into woody tissues (40) (*e.g.*, Giant sequoia, *Sequoiadendron giganteum*; Fig 5). As such, demographic performance in phanerophytes is likely more sensitive to the loss of individuals. Alternatively, hemicryptophytes typically undergo extreme annual shrinkage, and so their population structures typically change frequently over time (41). Accordingly, higher contribution ratios across hemicryptophytes and phanerophytes likely reflects the amount their population structure changes *vs.* their sensitivity to even just small changes in population structure.

Discussion

Linking demographic tools and conservation science

The stochastic nature of ecological systems (42), coupled with the rising prevalence of recurrent disturbance regimes (43), means that transient dynamics play a key role in determining near-term population forecasts (23, 44). Here, we emphasise how population structure has a substantial impact on the short-term dynamics of natural populations, and must therefore be explicitly accommodated within assessments of population viability (45). Specifically, the impacts of changes in population structure on demographic performance are of comparable magnitude to the effects of changing the fitness components of survival and fecundity rates, which underpin population viability (24, 28).

Documenting trends in population abundances is a key part of conservation science. Indeed, serving as the foundation for robust predictions of local (46) and global extinction risks (47), assessments of population size underpin three of the five criteria used in determining the IUCN Red List conservation status of species worldwide: ‘*High Decline Rate*’, ‘*Small Population Size and Decline*’ & ‘*Very Small Population Size*’ (48). A fourth criterion, ‘*Unfavourable Quantitative Analysis*’, then relates to estimating measures of demographic performance, which the IUCN recommends be done via population viability analyses (PVAs) (49). However, the utility of PVA frameworks for accurately predicting the trajectories of real-world systems is increasingly disputed (50). Moreover, these approaches frequently overlook transient dynamics and, crucially, the role of population structure in mediating population viability (Fig. 2A) (4, 51). Thus, although monitoring programs integrating population structure into assessments of species viability do exist (*e.g.*, NOAA’s Pacific salmon [*Oncorhynchus spp.*] monitoring service (52)), the inclusion of empirical records of population structure is not commonplace in biodiversity management and conservation. Hence, demonstrating the link between population structure and demographic performance, as we do here, offers a valuable platform for translating demographic modelling outputs into comprehensible applied insights for enhancing management predictions (11). Equally, highlighting the relevance of contributions of population structure to demographic performance, emphasises the value of adopting adaptive strategies to manage population structure in order to elicit its cascading effects on the dynamics of populations (32).

Linking population structure and life-history variation

We find that the value of population structure increases in species with faster life-history strategies. Specifically, contributions from changes in population structure to variance in short-term demographic performance are greater in populations with shorter generation times and/or whose investments into survival during earlier life stages are lower. These characteristics are indicative of faster life-history strategies (53, 54), thus, our findings highlight the particularly high value of population structure for informing the near-term forecasts and conservation of faster-lived species. With generation time and lifespan also linked to extinction risk (48, 55) and adaptability (56), the relationship between the importance of changes in population structure to short-term population dynamics and generation time compounds the importance of considering population structure as part of ongoing biodiversity conservation efforts.

Our findings also suggest that temporal, spatial, and/or experimental comparisons of populations possessing intermediate generation times report the highest variance in short-term demographic performance; a pattern that persists irrespective of the populations position along the second component axis (Fig. 2B). Although, short-lived species are expected to perform well in environments characterised by random stochastic variability (i.i.d.) (57), their fitness is expected to decline relative to that of long-lived species as stochastic variability becomes increasingly autocorrelated over time (58). Subsequently, although mediated by the type of stochasticity imposed, populations with both high and low generation times display an apparent capacity for buffering their dynamics against increased environmental stochasticity. As such, we might expect demographic performance in natural populations positioned more centrally on the generation time scale to be more labile in response to environmental variability. However, faster-lived species (*i.e.*, shorter-generation times) typically display more labile responses to environmental stochasticity, with the dynamics of slower-lived species (*i.e.*, shorter-generation times) more buffered against stochasticity (59). Accordingly, our findings here hint at how it is the cumulative effect of a species or populations suite of life-history strategies alongside its relative generation time that informs its overall response to environmental stochasticity. Interestingly, we report the population comparisons exhibiting greater variation in demographic performance to align along an axis associated with contributions from the interaction between population structure and vital rates to demographic performance (σ:γ:ϕ:$\boldsymbol{n}$). This axis describes a gradient from negative contributions of σ:γ:ϕ:$\boldsymbol{n}$ acting to diminish observed variance in short-term demographic performance, to positive contributions of σ:γ:ϕ:$\boldsymbol{n}$ that amplify observed variance. Regardless of these effects, populations that possess intermediate generation times appear less able to buffer their demographic performance against temporal, spatial, or experimentally imposed variability.

We also show how differences in plant growth form offer a nuanced understanding of the relationships between life-history traits and drivers of short-term demographic performance. For instance, we show how populations of slow growing woody phanerophytes (*e.g.*, Sugar maple, *A. saccharum*), who are sensitive to the loss of individuals (60), and populations of hemicryptophytes (*e.g.*, Silky oat-grass, *Danthonia sericea*), whose individuals annually recede back to ground level over winter, both exhibit greater contributions from their population structure to their demographic performance. One argument to explain these nuances relates to the mathematical pipeline underlying tLTRE analyses (4). Specifically a tLTRE is concerned with the sensitivity of short-term demographic performance to underlying population characteristics as well as the magnitude of any observed changes in said underlying characteristics (4). However, similar patterns have also been reported in the contributions of transient dynamics to the realised demographic performance of plant populations, with greater contributions from transient dynamics observed in plant species positioned at the extremities of life-history complexity (23, 51). Thus transient potential is larger in populations of trees and monocarpic plants (*i.e.*, plants that flower and produce seeds only once in their lifetime) than perennial herbs and shrubs (51). Although not wholly aligned with Raunkiær's growth form classifications, many monocarpic species are also considered hemicryptophytes (61). Thus, our observation here of congruent patterns in the demographic profiles of phanerophyte and hemicryptophyte plant species aligns with this previous evidence (51). The community contexts of many phanerophyte and hemicryptophyte species places a strong selective pressure on them producing many viable offspring to maximise their colonisation potential. A process that in turn elevates their transient potential (51). Hemicryptophytes include many early-successional plant species, who benefit from being able to anticipate and quickly monopolise available resources (62, 63). Meanwhile, although late-successional, many tree species exist within dense forest ecosystems, and need to take advantage of erratic canopy gap dynamics (64). Thus, the short-term demographic performance of both phanerophyte and hemicryptophyte species may indeed be similarly reliant on the contributions of changes in their population structure.

Caveats and cautions

The life-history trait space represented by our study sample is not exempt of spatial and taxonomic biases, with the majority of species represented comprising herbaceous perennials (*i.e.*, plants that do not develop woody tissues and typically reach reproductive maturity within a few years or less before losing their aboveground biomass during overwintering) studied in North America and Europe (65) (Fig. S1). Having shown how growth form and life-history variation correlate with the contributions of population structure to demographic performance, it is important to consider how the traits and growth forms of species not included could affect the patterns we observed. For instance, our sample lacks species possessing both long generation times and delayed ages at maturity (*e.g.*, Hoop pine, *Araucaria cunninghamii*) (27). Disturbance events associated with impacts on the structures and/or vital rates of plant populations are also not distributed equally across the globe. For instance, shifts in climatic regimes associated with changes to plant vital rates will likely be most acute in already highly arid and humid environments (66). Meanwhile, hotspots of deforestation, that directly affect the structure of affected tree populations, are found in South America and Asia (67), two areas for which we have limited data linking population structure and demographic performance (Fig. S1). Thus, continued efforts to understand how the interactions between population structure and vital rates informs demographic performance should focus on regions where the impacts of disturbances select for differing responses in population vital rates *vs.* population structure.

The findings we present here are not sensitive to the pooling of temporal, spatial and/or experimental comparisons across our data sample (Appendix S4). However, space-for-time substitutions have been criticised in ecology, as species do not necessarily respond to spatial climatic variation in the same way as they do to temporal shifts (68). One distinction in responses is likely due to the accumulation of impacts accrued whilst responding to temporal shifts over time (69), and the notion that future climate conditions will differ from those contemporary populations have experienced before (70). Alternatively, spatial comparisons likely involve comparisons among different populations who may have acclimatized to subtly different conditions over time.

Our dataset offers the largest scale of demographic data available to date linking associated changes in population vital rates and structure across time, space, and/or experimental treatments. Past synthesis work has demonstrated how COMPADRE (22), from which we sourced our data, and COMADRE (71) together contain over 1,600 temporal, spatial, and/or experimental comparisons of animal and plant population dynamics (72). Further explorations of these relationships are currently hindered by the lack of data explicitly detailing population structure across those studies (73). Considering the importance of population structure in determining short-term population dynamics, as we have shown here, we encourage authors to make population structure data publicly available, and for future efforts to quantify and assess population viability to capitalise on this key information.

Conclusions

Using 268 comparisons of population dynamics in 56 plant species across differing time periods, locations, and/or experimental treatments, we comprehensively assessed how population structure informs demographic performance across axes of life-history variation. Past theoretical work based on simplified population simulations evidenced a link between life-history variation and the contributions of population structure to variation in demographic performance (4). Yet, until now, we have lacked a robust empirical understanding of how population structure shapes population viability (13). Here, we demonstrate that the contributions of population structure to realised demographic performance are comparable to the effects of more routinely assessed patterns in population vital rates. As such, we illustrate the limitations of widespread practices assigning conservation statuses or offering forecasts of population dynamics in the absence of data describing population structure. We also highlight how life-history strategies and plant growth forms can modulate the impacts of population structure on demographic performance. With robust population forecasts requiring an appreciation for the nuanced interplay between a population's structure and its vital rates (11, 74), we encourage monitoring efforts to adopt approaches facilitating the streamlined integration of empirical records of population structure into viability assessments, or at the very least, appropriate usage of data integration to estimate latent population structure and its impact on population viability (11, 75). For instance, combining remote sensing technologies with semi-automated image segmentation can provide extensive records linking the structure and vital rates of plant (76, 77) and animal populations (78). Indeed, effectively managing and conserving global biodiversity warrants continued efforts to understand how population structure mediates demographic performance.

Methods

We developed a comparative framework using transient Life Table Response Experiments (tLTREs) (*sensu* (4)) to test our five hypotheses. Briefly, our approach comprised the following steps: (a) sourcing suitable structured population models, (b) quantifying life-history traits, (c) implementing tLTREs, (d) determining the strength of phylogenetic ancestry across sources of variance in population growth rates, and (e) assessing the association between axes of life-history variation and the relative contribution of population structure and vital rates to non-stable population growth rates. We carried out all analyses in *R* (79), and our fully commented scripts are publicly available on Zenodo (https://doi.org/10.5281/zenodo.15600668).

Sourcing population models

We tested our hypotheses using a sample of structured population models representing the dynamics of different plant populations sourced from the COMPADRE Plant Matrix Database (version 6.23.5..0; (22)). COMPADRE contains almost 9,000 matrix population models (MPMs) detailing survival, development (growth & shrinkage), and fecundity patterns across the life cycles of ~790 plant species. This information has been compiled from mostly (>98%) peer-reviewed publications addressing various research questions (65).

We derived our sample of MPMs from an initial collection of 2,217 MPMs representing 212 plant species. This initial collection comprised sets of structured population models originally screened for LTRE testing used to illustrate the exactLTRE methodology (72). Briefly, this screening entailed a series of selection criteria. First MPMs were confirmed as ergodic, primitive, and irreducible, to ensure they contain direct or indirect transition pathways between all life cycle stages and thus possessed a single dominant eigenvalue (80). Second, MPMs comprising fewer than three life stages were rejected, as lower-dimensional MPMs provide unreliable representations of population dynamics (81). Third, accepted MPMs described annual census periodicities and were from studies that parameterised multiple MPMs for their focal species/population. This step ensured consistent time intervals and that we could compare between MPMs representing the dynamics of a species or population compared over different time periods (*e.g.*, (82)), sites (*e.g.*, (83)), or experimental treatments (*e.g.*, (84)). Fourth, accepted MPMs contain no records of clonal reproduction because inconsistencies in the distinction between genets and ramets (*i.e.*, colonies *vs.* clones) across studies can lead to unreliable comparisons of population growth rates. Fifth, accepted MPMs also contained no life-cycle transitions that had not been observed empirically or that represented post-hoc manipulations of observed data, such that no transitions had been observed once and assumed to be constant across all replicates (time, sites, or treatments). Each accepted MPM was also meticulously screened for common life-cycle errors identified in Kendal *et al*. (85). Finally, accepted MPMs were required to have been digitised into COMPADRE alongside three sub-matrices (***U***, ***F**, and* ***C***), allowing for the life cycle transitions it describes to be decomposed into the processes of survival (***U***), reproduction (***F***), and asexual propagation (***C***) (Eq. 1).

$$A = U + F + C \qquad (1)$$

Here, from this initial collection of 2,217 MPMs, we specifically retained only models for which corresponding population vectors were available, either via publication in the original sources or because we obtained them via direct requests to authors. These population vectors detail the observed distributions of individuals across each life-stage (*i.e*., state distribution). This step allowed us to link population vectors documented during demographic census to the corresponding MPM describing the associated stage-specific vital rates. As such, we partitioned sources of variance in observed population growth rates into contributions from population structure and vital rates. Following this second screening phase, we retained 845 MPMs representing 56 plant species across 268 populations suitable for tLTRE decomposition (Table S1). This final sample comprised sets of MPMs originating from various comparisons of plant population dynamics across time, space, or experimental treatments, or combinations of these cases (Table S1). However, our comparisons across these different dimensions are justified, as our findings are not sensitive to the pooling of comparisons of population dynamics made across time, space, or experimental treatments (Appendix S4).

Estimating tLTRE contributions

Testing each of our hypotheses necessitated quantifying the relative contribution of changes in population structure to observed variation in demographic performance across comparisons of plant population dynamics. For this step, we implemented tLTRE analyses using a modified version of the recently developed exactLTRE framework (72). Classical LTRE analysis quantifies the contributions to any observed variation in long-term (*i.e.* asymptotic) population growth rates (λ) affected by changes in particular MPM elements across a collection of models (86). However, due to their basis in Taylor Series approximation, classical LTRE approaches provide only an approximation of the contribution of vital rate changes to variation in λ (72). The exactLTRE framework uses a functional analysis of variance (fANOVA; (87, 88)) approach to avoid this approximation, accurately partitioning observed variance in demographic performance across both the main effects of survival, development, and fecundity, and the interactions between these vital rates (72). Here, to assess the contribution of changes in population structure, alongside changes in survival, development, and fecundity, to variation in realised (*i.e.* transient) population growth rates ($\lambda_{\text{transient}}$), we modified the functionality of the *exactLTRE* R package (89). Specifically, this modification allowed for partitioning observed variance in $\lambda_{\text{transient}}$ across the main and interaction effects of changes in population vital rates and age/stage structure. We note, that efforts are ongoing to add these modified functions to future versions of *exactLTRE*, to promote tLTRE tools.

We ran tLTRE analyses across our sample of 268 population comparisons. First, across each comparison, we computed $\lambda_{\text{transient}}$ for each population replicate (x) using their associated MPM ($\boldsymbol{A}_x$) and population vectors ($\boldsymbol{n}_x$) (Eq. 2). This metric indicates retrospectively whether the size of the population grew, remained constant, or declined ($\lambda_{\text{transient}} > 1, = 1, < 1$, respectively) over a single time interval.

$$\lambda_{transient} = \frac{\Sigma A_x n_x}{\Sigma n_x} \quad (2)$$

Next, we calculated the variance across the sequence of $\lambda_{transient}$ estimates obtained for each population replicate [$var(\lambda_{transient})$]. Typically, variance is calculated as the sum of the squared deviations divided by N - 1, where N is the sample size. However, this approach assumes an incomplete sample. Instead, when computing $var(\lambda_{transient})$, our use of the fANOVA framework assumes that we possess the complete sample of $\lambda_{transient}$ estimates. As such, our estimates of $var(\lambda_{transient})$ are equal to the mean of the squared deviations across each population.

After calculating $var(\lambda_{transient})$ for each population comparison, we decomposed the source of this variance into the relative contributions of any changes observed across their associated sequences of ***A*** and ***n*** products. By way of a walkthrough our exact decomposition approach, consider the following population, whose dynamics and population structure were censused across two separate scenarios (x and $x+1$):

$$A_x = \begin{bmatrix} 0.2 & 2.0 \\ 0.3 & 0.5 \end{bmatrix} \ \& \ n_x = \begin{bmatrix} 0.6 \\ 0.4 \end{bmatrix} \quad A_{x+1} = \begin{bmatrix} 0.2 & 1.5 \\ 0.7 & 0.5 \end{bmatrix} \ \& \ n_{x+1} = \begin{bmatrix} 0.2 \\ 0.8 \end{bmatrix}. \quad (3)$$

Accordingly, we possess a sequence of two ***A*** and ***n*** products for this population, with $var(\lambda_{transient})$ across these replicates estimated to be 0.0576 ($\lambda_{transient}$: x = 1.3 & x+1 = 1.78). We then compute the mean MPM ($\underline{\boldsymbol{A}}$) and population vector ($\underline{\boldsymbol{n}}$) (arithmetic element-by-element means, in each case) represented by our observed ***A*** and ***n*** products:

$$\underline{A} = \begin{bmatrix} 0.2 & 1.75 \\ 0.5 & 0.5 \end{bmatrix} \ \& \ \underline{n} = \begin{bmatrix} 0.4 \\ 0.6 \end{bmatrix}. \quad (4)$$

Next, holding all matrix elements and/or ***n*** at their mean condition, we systematically replace the value of each matrix element, a_{ij}, and the population vector, ***n***, with their observed conditions across our sequence of ***A*** and ***n*** products. We then recalculate the $\lambda_{transient}$ estimates associated with these perturbed $\boldsymbol{A}$ and $\boldsymbol{n}$ products ($\boldsymbol{A}^{pert}$ and $\boldsymbol{n}^{pert}$) before recalculating the variance across these modified $\lambda_{transient}$ estimates. In our hypothetical population, matrix elements $a_{2,1}$ and $a_{1,2}$, and $\boldsymbol{n}$ exhibit different conditions over time. Subsequently, we are only interested in how the changes in these three entities contribute to $var(\lambda_{transient})$. To quantify the main (first-order) effects of each entity, we isolate the independent changes observed in each entity whilst holding all other values at their mean condition (Eqs. 5-7), before then computing the variance associated with only these imposed modifications.

$$A_{x}^{pert} = \begin{bmatrix} 0.2 & 2.0 \\ 0.5 & 0.5 \end{bmatrix} \; \& \; \underline{n} = \begin{bmatrix} 0.4 \\ 0.6 \end{bmatrix} \quad A_{x+1}^{pert} = \begin{bmatrix} 0.2 & 1.5 \\ 0.5 & 0.5 \end{bmatrix} \; \& \; \underline{n} = \begin{bmatrix} 0.4 \\ 0.6 \end{bmatrix} \tag{5}$$

$$A_{x}^{pert} = \begin{bmatrix} 0.2 & 1.75 \\ 0.3 & 0.5 \end{bmatrix} \; \& \; \underline{n} = \begin{bmatrix} 0.4 \\ 0.6 \end{bmatrix} \quad A_{x+1}^{pert} = \begin{bmatrix} 0.2 & 1.75 \\ 0.7 & 0.5 \end{bmatrix} \; \& \; \underline{n} = \begin{bmatrix} 0.4 \\ 0.6 \end{bmatrix} \tag{6}$$

$$\underline{A} = \begin{bmatrix} 0.2 & 1.75 \\ 0.5 & 0.5 \end{bmatrix} \; \& \; n_{x}^{pert} = \begin{bmatrix} 0.6 \\ 0.4 \end{bmatrix} \quad \underline{A} = \begin{bmatrix} 0.2 & 1.75 \\ 0.5 & 0.5 \end{bmatrix} \; \& \; n_{x}^{pert} = \begin{bmatrix} 0.2 \\ 0.8 \end{bmatrix} \tag{7}$$

In equation 5, we focus on the effect of changes in matrix element $a_{2,1}$. Here, the $\lambda_{transient}$ values for the two scenarios presented are 1.78 & 1.48, respectively, such that the recorded changes in element $a_{2,1}$ contribute to an observed $var(\lambda_{transient})$ of 0.0225. Meanwhile, the recorded changes in element $a_{1,2}$ (equation 6) contribute an observed $var(\lambda_{transient})$ of 0.0064 ($\lambda_{transient}$: $x = 1.55$ & $x+1 = 1.71$), while changes in $\boldsymbol{n}$ (equation 7) contribute an observed $var(\lambda_{transient})$ of 0.0961 ($\lambda_{transient}$: $x = 1.32$ & $x+1 = 1.94$). Repeating the above steps for different combinations of the focal entities then allows for quantifying the contributions of interactions between multiple changing entities to $var(\lambda_{transient})$ (72); for instance, the effects of simultaneous changes to the population vector ($\boldsymbol{n}$) and element $a_{1,2}$ of matrix $\boldsymbol{A}$ on $var(\lambda_{transient})$ constitutes an interaction effect.

After identifying the contributions of different matrix elements, to compare contributions from population structure to those of the vital rates of survival (σ), development (γ), and fecundity

(ϕ) (*H1*), we then determined which vital rate each matrix element corresponded to. For fecundity, this step simply involved summing the contributions of matrix elements only detailing per-capita fecundity rates, which we identified using each population's reproductive sub-matrix (***F***; Eq. 1). For survival and development, we first determined the matrix elements corresponding with stasis (*i.e.*, individuals remaining within a life-stage from *t* to *t*+1), stage progression (*i.e.*, growth/development), and stage retrogression (*i.e.* shrinkage/de-development). Next, for matrix elements describing progression and retrogression, we determined the proportion of each element associated with survival (P_{σ}) and development (P_{γ}; growth and shrinkage pooled). Dividing each matrix element by its corresponding stage-specific survival, the column-sum of the population's survival sub-matrix (***U***), we extracted the population's survival-independent progression/retrogression matrix (***U'***). We then quantified survival contributions to $var(\lambda_{transient})$ by totalling the contributions of matrix elements associated with stasis and the contributions of matrix elements associated with development weighted by P_{σ}. For the contributions of development to $var(\lambda_{transient})$, we summed the contributions of matrix elements associated with development weighted by P_{γ}. Finally, we summed the contributions to $var(\lambda_{transient})$ arising from second-order interactions between different entities, categorising only whether they involved interactions between just vital rates or between vital rates and population structure.

Finally, we standardised our contribution estimates to ensure comparability across populations displaying a range of magnitudes in $var(\lambda_{transient})$. Specifically, we translated our estimates of contribution from survival (σ), development (γ), fecundity (ϕ), population structure (***n***), and their interaction effects (σ:γ:ϕ:***n*** & σ:γ:ϕ) to observed variance in $\lambda_{transient}$ into proportional effects. For each population set, combining the absolute values of contributions of survival, development, fecundity, and population structure $var(\lambda_{transient})$ provided us with a total contribution estimate (C_{total}) whilst accommodating for both negative and positive contribution patterns. Subsequently, we separately quantified the directional proportional effects of survival, development, fecundity, population structure, and their interaction effects (C_i) as C_i/C_{total}. We then calculated a contribution ratio for each population comparison (C_{ratio}), equal to the summed contributions of population structure ($\boldsymbol{n}$) and the interaction between population structure and vital rates (σ:γ:ϕ:$\boldsymbol{n}$) divided by the summed contributions of survival (σ), development (γ), fecundity (ϕ), and their interactions (σ:γ:ϕ). Accordingly, a ratio of one implies a balanced contribution of population vital rates *vs*. population structure, with higher estimates inferring a greater influence from the population structure. Finally, following our computation of these proportional effects, to mitigate for skewed distirubtions we omitted all estimates outside the 90th percentiles of our $var(\lambda_{transient})$ and contribution variables.

Quantifying life-history variation

Testing our hypotheses required quantifying life-history trait variation across our population comparison sample. For each population comparison, we estimated the mean MPM (*i.e.,* the element-by-element arithmetic mean) from the associated set of MPMs describing the focal species/population dynamics across different time intervals, locations or experimental treatments. Next, with life-history trait estimates obtained from MPMs sensitive to matrix dimensionality (90), we collapsed each mean MPM into a 3 × 3 matrix to ensure comparability across populations and species. Using the matrix collapsing function *mpm_collapse* of the *Rcompadre* R package (91), we condensed together any life stages beyond the second life stage into a single terminal stage while keeping the first two stages unaltered. This approach retains the original eigen-structure of the original MPM (92); thereby minimising the impact on any subsequent measures derived from the collapsed MPMs. Using age-from-stage approaches (34, 93) on our collapsed mean MPMs, we then computed life-history traits routinely used to describe how individuals invest differentially into survival, development, and reproduction (24, 28).

Whilst many life-history traits can be obtained from MPMs (91), our hypotheses focused on selected trait measures (Table 1). To evaluate how contributions from changes in population structure vary across the fast-slow continuum of life-history strategies (*H2*), we focused on the selected traits of generation time (T), age at reproductive maturity (L_{α}), mean life expectancy (η_e), and reproductive window ($L_{\alpha\text{-}\omega}$). Our rationale for selecting these metrics is that they all possess the same units (time) and thus allow for cross-species comparisons while avoiding artifactual patterns that can emerge from mixing life-history traits with different units (36). Meanwhile, to explore the relationship between contributions from variation in population structure and patterns in population life cycle survival profile ($\Delta\sigma$) (*H3*), we calculated the slope coefficient of a linear regression model fitted to the sequence of mean stage-specific survival probabilities obtained for each population comparison (*e.g.*, slope of survival across life stages; see Appendix S3 for details on the validity of this approach). Consequently, positive values reflect an increasing likelihood of survival as individuals progress through their life cycle. To ensure this assessment accounted for the effect of lifetime survival (*i.e.*, fast *vs*. slow) on the relationship between sources of variance in demographic performance and life cycle survival profile, we also computed a measure of mean lifetime survival ($\underline{\sigma}$) associated with each population comparison. Mean lifetime survival was equal to the grand mean of mean stage-specific survival probabilities obtained for each population comparison. Finally, to assess how contributions from changes in population structure align with reproductive trait variation (*H4*), we used the measure of degree of iteroparity (S). This dimensionless measure of entropy (94) reflects the reproductive parity continuum, delineating species based on the timing and frequency of their reproductive investments (27). After obtaining estimates for each selected life-history trait, we omitted all estimates outside the 90th percentiles of each variable (estimates which were later replaced using phylogenetic imputation, see *Establishing phylogenetic relationships*).

Establishing phylogenetic relationships

Comparative assessments of demographic and life-history trait variation need to consider non-random patterns of variance-covariance across populations based on shared phylogenetic ancestry (95). To further compare patterns in the contribution of population structure to $var(\lambda_{transient})$ *vs.* those of the vital rates of survival, development, and fecundity (*H1*), we sought to test the strength of phylogenetic signal across our contributional effect variables. Thus, we computed the phylogenetic distances between the 56 species represented across our LTRE comparison sample. We sourced unique identifier codes for each species from the Open Tree of Life (OTL) (taxonomy version 3.6; (96)) to construct a species-level phylogenetic subtree using the *phytools* (97) and *ape* R packages (98). We then computed branch lengths for our species-level phylogenetic subtree using Grafen's computation method (99), ensured our subtree contained a single common ancestor, and removed any polytomies (≥ 3 species emerging from a single origin).

Next, we used our species-level phylogenetic subtree to impute any missing or omitted estimates across our vital rate and life-history measures, enabling us to retain details from all populations across our sample. We used the *phylopars* function from the *Rphylopars* package

(100) to impute missing values (assuming a Brownian Motion evolutionary model) across our demographic and life-history measures. 2.7% of our final data sample was generated using phylogenetic imputation, and we ran sensitivity tests confirming that our results are insensitive to this imputation (Appendix S5).

Finally, to further assess how the contribution of population structure to $var(\lambda_{transient})$ compares to those of the vital rates of survival, development, and fecundity (*H1*), we tested the strength of phylogenetic signal across our contributional effect variables. After using our species-level subtree to impute missing data, we expanded subtree branch tips for species replicates across our population sample (48 of 56 species), generating a population-level phylogenetic subtree. Carrying out this branch expansion involved rooting replicate instances of the same species onto the species' corresponding branch tip in our species-level subtree. When rooting replicate entries, we ensured each replicate was separated by branch lengths of infinitesimal distances (ε = 0.0000001 units). This step ensured that populations of the same species were considered very closely related, preventing the introduction of polytomies. Recent work using the same demographic data has demonstrated that the order in which population replicates are added to population-level phylogenetic trees does not affect transient metrics (101). The exact population-level subtree we used in this study is available on Zenodo (https://doi.org/10.5281/zenodo.15600668). Using this population-level subtree, we estimated phylogenetic signal using Pagel's Λ (33) via the *caper* package (102). Pagel's Λ ranges between 0 to 1 depending on whether attribute estimates vary randomly (Pagel's $\Lambda \approx 0$) or are more similar across more closely related species (Pagel's $\Lambda \approx 1$) (35).

Linking tLTRE contributions and life-histories

To test whether the contributions to $var(\lambda_{transient})$ from changes in population structure are greater in species with faster life-histories (*H2*), we carried out a phylogenetically weighted partial least squares analysis (pPLS). Specifically, we used pPLS to assess the relationship between our proportional effects variables and the life-history traits of generation time (T), age at reproductive maturity (L_{α}), mean life expectancy (η_e), and reproductive window ($L_{\alpha\text{-}\omega}$). Prior to this pPLS we transformed our life-history trait estimates to ensure normal distributions, applying log-transformations to our estimates of generation time (T), age at reproductive maturity (L_{α}) (both $log(x)$), and reproductive window ($L_{\alpha\text{-}\omega}$) ($log(x+5)$), and an inverted power-transformation to our mean life expectancy estimates (η_e) ($-x^{-0.275}$). To account for the influence of body size on the development of life-history traits (24), we then scaled our transformed life-history variables according to a measure of adult plant height assigned to each species (27). We attributed each plant species a height class corresponding with their Raunkiær growth form classification (40), which catalogues plant species according to the extent to which their apical meristems (*i.e.*, renewal buds) recede to ground level during periods of unfavourable growing conditions. Synthesising details of the Raunkiær growth form classification of different plant species from the TRY database (103) and Plants of the World Online (104), we grouped our plant species into one of seven Raunkiær growth form classes that subsequently defined their associated height (m): (i) geophytes [-0.25m]; (ii) hemicryptophytes [0m]; (iii) chamaephytes [0.25m]; (iv) epiphytes [4m]; (v) nanophanerophytes [2m]; (vi) mesophanerophytes [8m]; and (vii) megaphanerophytes [30m] (See (27) for further details). To scale our life-history traits according to size, we retained the residuals from linear models of the relationship between each life-history trait and the height class estimates attributed to each species. Next, following (105), we transformed all our pPLS variables according to their phylogenetic weighting, using a phylogenetic variance-covariance matrix generated from our population-level phylogenetic subtree. We then implemented our pPLS using the *plsdepot* R package (106) before imposing a varimax rotation upon the multivariate parameter space using the *GPArotation* package (107). We performed varimax rotation to ensure that our life-history variables were better aligned with the main axes of the parameter space (108); a common approach used to improve the interpretation of multivariate analysis outputs (109).

To test (*H3*) whether the importance of contributions from variation in population structure to $var(\lambda_{transient})$ correlates with the life cycle survival profiles of natural populations, we used phylogenetically-corrected Bayesian multilevel modelling. To do so, and following the approach described above, we first scaled our measure of life cycle survival profiles ($\Delta\sigma$) according to the plant size estimates associated with assigned Raunkiær growth form classifications. Using the *brms* R package (110), we then modelled the relationship between our log-transformed C_{ratio} ($log(x+0.01)$) and the additive effects of our scaled $\Delta\sigma$ and $\underline{\sigma}$ estimates using a model fitted with default priors. When extracting outputs from this model we set $\underline{\sigma}$ to its median value observed across our sample, allowing us to eliminate the time-dimension from each survival profile, to focus instead on the shape of survival through the life-cycle (111). To test (*H5*) how growth form mediates any observed patterns between sources of variance in $\lambda_{transient}$ and their life-history traits, this model also included assigned Raunkiær growth form classification as a fixed effect variable. Note, due to limited sample sizes in our geophyte (n = 4), nanophanerophyte (28), mesophanerophyte (28), and megaphanerophyte (6) Rankiær classes, we pooled geophytes with hemicryptophytes and collapsed nano-, meso-, and megaphanerophytes together as phanerophytes. Thus, growth form was a fixed effect variable comprised of four classes (chamaephytes [n = 45], hemicryptophytes [144], epiphytes [17], and phanerophytes [62]). Our *brms* model also included a grouping term to account for variance-covariance among our 268 populations across 56 species according to the branch lengths outlined in our phylogenetic subtree. To ensure we selected the most appropriate model, we initially applied both linear and polynomial functions of explanatory variables to our model before determining a linear function to be the best model fit using leave-one-out comparison (LOO) (LOO weights: Linear = 0.999; Polynomial < 0.001). We ran our model over four Markov Chains, each consisting of 3,000 iterations, extracting the predicted effects of $\Delta\sigma$ on C_{ratio} across growth forms, when $\underline{\sigma}$ is held at its median value.

To test (*H4*) whether the relative importance of contributions from population structure to $var(\lambda_{transient})$ decreases with increasing iteroparity, we again used a phylogenetically-corrected Bayesian multilevel model fitted using default priors. Specifically, we modelled the relationship between our log-transformed C_{ratio} and power-transformed ($x^{0.35}$) degree of iteroparity (S) variables. As before, we scaled degree of iteroparity according to plant size and included a phylogenetic grouping term within our model to account for variance-covariance between populations/species. We also, again, included Raunkiær growth form classification as a fixed effect variable, to test (*H5*) how growth form mediates any observed patterns between sources of variance in $\lambda_{transient}$ and their life-history traits. We preliminarily fitted both linear and polynomial functions to assess model fit before using LOO comparisons to identify that the linear model provided the best representation of our data (LOO weights: Linear = 0.718; Polynomial = 0.282). We once again implemented our model over four Markov Chains (3,000 iterations each) and extracted the predicted effects of S on C_{ratio}.

Acknowledgements

J.C. and C.H. were supported by a NERC Pushing the Frontiers grant (NE/X013766/1) to R.S.G., I.S. & A.H.. C.H. was also partly supported by a Marie Curie Fellowship (MSCA DensPopDy #10115386) with funding through UKRI (EP/Z002826/1), hosted by R.S.G. M.Q. was supported by a Marie Curie Fellowship (MSCA TraitMatter #101146302) with funding through UKRI (EP/Z00232X/1), hosted by R.S.G. DJH was supported by the University of Exeter; DNK was supported by a Fulbright award to the University of Exeter.

References

1. W. F. Morris, D. F. Doak, *Quantitative conservation biology: Theory and practice of population viability analysis* (Sinauer Associates, Inc., 2002).

2. A. Hastings, *et al.*, Transient phenomena in ecology. *Science* **361**, 1–9 (2018).

3. P. Capdevila, I. Stott, M. Beger, R. Salguero-Gómez, Towards a comparative framework of demographic resilience. *Trends Ecol. Evol.* **35**, 776–786 (2020).

4. D. N. Koons, D. T. Iles, M. Schaub, H. Caswell, A life-history perspective on the demographic drivers of structured population dynamics in changing environments. *Ecol. Lett.* **19**, 1023–1031 (2016).

5. A. A. Maldonado-Chaparro, D. T. Blumstein, K. B. Armitage, D. Z. Childs, Transient LTRE analysis reveals the demographic and trait-mediated processes that buffer population growth. *Ecol. Lett.* **21**, 1693–1703 (2018).

6. F. S. Dobson, *et al.*, The Demographic Basis of Population Growth: A 32-Year Transient Life Table Response Experiment. *Ecol. Lett.* **27**, e14512 (2024).

7. S. R. Hoy, *et al.*, Fluctuations in age structure and their variable influence on population growth. *Funct. Ecol.* **34**, 203–216 (2020).

8. B. Sommer, *et al.*, Decadal demographic shifts and size-dependent disturbance responses of corals in a subtropical warming hotspot. *Sci. Rep.* **14** (2024).

9. V. Radchuk, C. Turlure, N. Schtickzelle, Each life stage matters: the importance of assessing the response to climate change over the complete life cycle in butterflies. *J. Anim. Ecol.* **82**, 275–285 (2013).

10. T. Coulson, *et al.*, Age, Sex, Density, Winter Weather, and Population Crashes in Soay Sheep. *Science* **292**, 1528–1531 (2001).

11. D. N. Koons, T. W. Arnold, M. Schaub, Understanding the demographic drivers of realized population growth rates. *Ecol. Appl.* **27**, 2102–2115 (2017).

12. S. Jenouvrier, Impacts of climate change on avian populations. *Glob. Change Biol.* **19**, 2036–2057 (2013).

13. E. E. Crone, *et al.*, How do plant ecologists use matrix population models? *Ecol. Lett.* **14**, 1–8 (2011).

14. D. Gibson, T. W. Arnold, F. E. Buderman, D. N. Koons, Explaining the divergence of population trajectories for two interacting waterfowl species. *Ecol. Monogr.* **95**, e1642 (2025).

15. A. Hastings, Transients: The key to long-term ecological understanding? *Trends Ecol. Evol.* **19**, 39–45 (2004).

16. T. H. G. Ezard, *et al.*, Matrix models for a changeable world: The importance of transient dynamics in population management. *J. Appl. Ecol.* **47**, 515–523 (2010).

17. M. Christian, W. C. Oosthuizen, M. N. Bester, P. J. N. de Bruyn, Robustly estimating the demographic contribution of immigration: Simulation, sensitivity analysis and seals. *J. Anim. Ecol.* **93**, 632–645 (2024).

18. J. Summers, E. J. Cosgrove, R. Bowman, J. W. Fitzpatrick, N. Chen, Density dependence maintains long-term stability despite increased isolation and inbreeding in the Florida Scrub-Jay. *Ecol. Lett.* **27**, e14483 (2024).

19. C. R. Nater, *et al.*, Spatial consistency in drivers of population dynamics of a declining migratory bird. *J. Anim. Ecol.* **92**, 97–111 (2023).

20. S. Tenan, D. Becker, D. Tolkmitt, M. Schaub, Decomposing fecundity and evaluating demographic influence of multiple broods in a migratory bird. *J. Anim. Ecol.* **90**, 1071–1084 (2021).

21. K. Layton-Matthews, *et al.*, Environmental change reduces body condition, but not population growth, in a high-arctic herbivore. *Ecol. Lett.* **24**, 227–238 (2021).

22. R. Salguero-Gómez, *et al.*, The COMPADRE Plant Matrix Database: An open online repository for plant demography. *J. Ecol.* **103**, 202–218 (2015).

23. J. L. McDonald, I. Stott, S. Townley, D. J. Hodgson, Transients drive the demographic dynamics of plant populations in variable environments. *J. Ecol.* **104**, 306–314 (2016).

24. S. C. Stearns, *The Evolution of Life Histories* (Oxford University Press, 1992).

25. A. Compagnoni, *et al.*, Herbaceous perennial plants with short generation time have stronger responses to climate anomalies than those with longer generation time. *Nat. Commun.* **12**, 1–8 (2021).

26. Leishman, M. R., Wright, I. J., Moles, A. T., Westoby, M., "The Evolutionary Ecology of Seed Size" in *Seeds: The Ecology of Regeneration in Plant Communities*, 2nd Edition, (CAB International, 2000).

27. R. Salguero-Gómez, *et al.*, Fast–slow continuum and reproductive strategies structure plant life-history variation worldwide. *Proc. Natl. Acad. Sci.* **113**, 220–235 (2016).

28. S. C. Stearns, Trade-Offs in Life-History Evolution. *Funct. Ecol.* **3**, 259–268 (1989).

29. J.-P. Desforges, *et al.*, Environment and physiology shape Arctic ungulate population dynamics. *Glob. Change Biol.* **27**, 1755–1771 (2021).

30. C. Stuligross, N. M. Williams, Past insecticide exposure reduces bee reproduction and population growth rate. *Proc. Natl. Acad. Sci.* **118**, e2109909118 (2021).

31. M. C. Allen, M. Clinchy, L. Y. Zanette, Fear of predators in free-living wildlife reduces population growth over generations. *Proc. Natl. Acad. Sci.* **119**, e2112404119 (2022).

32. M. Gamelon, *et al.*, Efficient use of harvest data: a size-class-structured integrated population model for exploited populations. *Ecography* **44**, 1296–1310 (2021).

33. M. Pagel, Inferring the historical patterns of biological evolution. *Nature* **401**, 877–884 (1999).

34. H. Caswell, *Matrix population models: Construction, analysis and interpretation* (Oxford

University Press Inc, 2001).

35. R. P. Freckleton, P. H. Harvey, M. Pagel, Phylogenetic analysis and comparative data: A test and review of evidence. *Am. Nat.* **160**, 712–726 (2002).

36. I. Stott, *et al.*, Life histories are not just fast or slow. *Trends Ecol. Evol.* **39**, 830–840 (2024).

37. T. Yamada, *et al.*, Strong habitat preference of a tropical rain forest tree does not imply large differences in population dynamics across habitats. *J. Ecol.* **95**, 332–342 (2007).

38. A. Jonsson, B. Ebenman, Are Certain Life Histories Particularly Prone to Local Extinction? *J. Theor. Biol.* **209**, 455–463 (2001).

39. M. Bogdziewicz, *et al.*, Evolutionary ecology of masting: mechanisms, models, and climate change. *Trends Ecol. Evol.* **39**, 851–862 (2024).

40. C. Raunkiaer, *The life forms of plants and statistical plant geography; being the collected papers of C. Raunkiaer.* (1934).

41. R. Salguero-Gómez, B. B. Casper, Keeping plant shrinkage in the demographic loop. *J. Ecol.* **98**, 312–323 (2010).

42. L. G. Shoemaker, *et al.*, Integrating the underlying structure of stochasticity into community ecology. *Ecology* **101**, e02922 (2020).

43. M. J. Emslie, *et al.*, Increasing disturbance frequency undermines coral reef recovery. *Ecol. Monogr.* **94**, e1619 (2024).

44. M. M. Ellis, E. E. Crone, The role of transient dynamics in stochastic population growth for nine perennial plants. *Ecology* **94**, 1681–1686 (2013).

45. M. Gamelon, *et al.*, Making use of harvest information to examine alternative management scenarios: a body weight-structured model for wild boar. *J. Appl. Ecol.* **49**, 833–841 (2012).

46. R. A. F. De Lima, *et al.*, Comprehensive conservation assessments reveal high extinction risks across Atlantic Forest trees. *Science* **383**, 219–225 (2024).

47. A. Dietzel, M. Bode, S. R. Connolly, T. P. Hughes, The population sizes and global extinction risk of reef-building coral species at biogeographic scales. *Nat. Ecol. Evol.* **5**, 663–669 (2021).

48. G. M. Mace, *et al.*, Quantification of extinction risk: IUCN's system for classifying threatened species. *Conserv. Biol.* **22**, 1424–1442 (2008).

49. IUCN Standards and Petitions Committee, Guidelines for Using the IUCN Red List Categories and Criteria. Version 16. *Prep. Stand. Petitions Comm.* (2024).

50. T. Coulson, G. M. Mace, E. Hudson, H. Possingham, The use and abuse of population viability analysis. *Trends Ecol. Evol.* **16**, 219–221 (2001).

51. I. Stott, M. Franco, D. Carslake, S. Townley, D. Hodgson, Boom or bust? A comparative analysis of transient population dynamics in plants. *J. Ecol.* **98**, 302–311 (2010).

52. E. R. Buhle, *et al.*, Using integrated population models to evaluate fishery and environmental impacts on Pacific salmon viability.

53. S. Hamel, *et al.*, Fitness costs of reproduction depend on life speed: empirical evidence

from mammalian populations. *Ecol. Lett.* **13**, 915–935 (2010).

54. J. Gaillard, *et al.*, Generation Time: A reliable metric to measure life-history variation among mammalian populations. *Am. Nat.* **166**, 119–123 (2005).

55. J. Staerk, *et al.*, Performance of generation time approximations for extinction risk assessments. *J. Appl. Ecol.* **56**, 1436–1446 (2019).

56. Pearson, R. G., *et al.*, Life history and spatial traits predict extinction risk due to climate change. *Nat. Clim. Change* **4**, 217–221 (2014).

57. S. D. Tuljapurkar, Population dynamics in variable environments. III. Evolutionary dynamics of *r*-selection. *Theor. Popul. Biol.* **21**, 141–165 (1982).

58. M. Paniw, A. Ozgul, R. Salguero-Gómez, Interactive life-history traits predict sensitivity of plants and animals to temporal autocorrelation. *Ecol. Lett.* **21**, 275–286 (2018).

59. Le Coeur, C., Yoccoz, N. G., Salguero-Gómez R., Vindenes, Y., Life history adaptations to fluctuating environments: Combined effects of demographic buffering and lability. *Ecol. Lett.* **25**, 2107–2119 (2022).

60. W. A. Hoffmann, Fire and population dynamics of woody plants in a neotropical savanna: Matrix model projections. *Ecology* **80**, 1354–1369 (1999).

61. K. E. Frankiewicz, *et al.*, Derived woodiness and annual habit evolved in African umbellifers as alternative solutions for coping with drought. *BMC Plant Biol.* **21**, 383 (2021).

62. M. Huston, T. Smith, Plant Succession: Life History and Competition. *Am. Nat.* **130**,

168–198 (1987).

63. D. Tilman, Constraints and Tradeoffs: Toward a Predictive Theory of Competition and Succession. *Oikos* **58**, 3–15 (1990).

64. T. C. Whitmore, Canopy Gaps and the Two Major Groups of Forest Trees. *Ecology* **70**, 536–538 (1989).

65. G. Römer, J. P. Dahlgren, R. Salguero-Gómez, I. M. Stott, O. R. Jones, Plant demographic knowledge is biased towards short-term studies of temperate-region herbaceous perennials. *Oikos* **2024**, e10250 (2024).

66. E. M. Fischer, U. Beyerle, R. Knutti, Robust spatially aggregated projections of climate extremes. *Nat. Clim. Change* **3**, 1033–1038 (2013).

67. S. L. Lewis, D. P. Edwards, D. Galbraith, Increasing human dominance of tropical forests. *Science* **349**, 827–832 (2015).

68. D. L. Perret, M. E. K. Evans, D. F. Sax, A species' response to spatial climatic variation does not predict its response to climate change. *Proc. Natl. Acad. Sci.* **121**, e2304404120 (2024).

69. J. Cant, *et al.*, Current estimates of population resilience do not predict resilience to directional environmental shifts. *BioRxiv* (2025).

70. G. Bell, Evolutionary rescue and the limits of adaptation. *Philos. Trans. R. Soc. B Biol. Sci.* **368**, 1–6 (2013).

71. R. Salguero-Gómez, *et al.*, COMADRE: A global data base of animal demography. *J.*

Anim. Ecol. **85**, 371–384 (2016).

72. C. M. Hernández, S. P. Ellner, P. B. Adler, G. Hooker, R. E. Snyder, An exact version of Life Table Response Experiment analysis, and the R package exactLTRE. *Methods Ecol. Evol.* **14**, 939–951 (2023).

73. S. J. L. Gascoigne, *et al.*, A standard protocol to report discrete stage-structured demographic information. *Methods Ecol. Evol.* **14**, 2065–2083 (2023).

74. E. White, *et al.*, Resilience of a long-lived mammal: time and demographic structure matter. [Preprint] (2025). Available at: https://www.authorea.com/users/879023/articles/1258323-resilience-of-a-long-lived-mammal-time-and-demographic-structure-matter?commit=402f9b0e343cea73d8dc9f9303885c8628ddb418 [Accessed 13 February 2025].

75. Oppel, S., *et al.*, Assessing population viability while accounting for demographic and environmental uncertainty. *Ecology* **95**, 1809–1818 (2014).

76. P. J. Olsoy, *et al.*, Demography with drones: detecting growth and survival of shrubs with unoccupied aerial systems. *Restor. Ecol.* **32**, e14106 (2024).

77. A. Rosen, *et al.*, Modelling forest dynamics using integral projection models (IPMs) and repeat LiDAR. [Preprint] (2025). Available at: http://biorxiv.org/lookup/doi/10.1101/2025.01.06.631514 [Accessed 4 June 2025].

78. T. C. Stone, K. J. Davis, Using unmanned aerial vehicles to estimate body volume at scale for ecological monitoring. *Methods Ecol. Evol.* **16**, 317–331 (2025).

79. R Core Team, R: A language and environment for statistical computing. (2022). Deposited 2022.

80. I. Stott, S. Townley, D. Carslake, D. J. Hodgson, On reducibility and ergodicity of population projection matrix models. *Methods Ecol. Evol.* **1**, 242–252 (2010).

81. D. N. Koons, J. B. Grand, B. Zinner, R. F. Rockwell, Transient population dynamics: Relations to life history and initial population state. *Ecol. Model.* **185**, 283–297 (2005).

82. T. Ticktin, R. Ganesan, M. Paramesha, S. Setty, Disentangling the effects of multiple anthropogenic drivers on the decline of two tropical dry forest trees. *J. Appl. Ecol.* **49**, 774–784 (2012).

83. S. Pisanu, E. Farris, R. Filigheddu, M. B. García, Demographic effects of large, introduced herbivores on a long-lived endemic plant. *Plant Ecol.* **213**, 1543–1553 (2012).

84. S. K. Ghimire, O. Gimenez, R. Pradel, D. McKey, Y. Aumeeruddy-Thomas, Demographic variation and population viability in a threatened Himalayan medicinal and aromatic herb Nardostachys grandiflora: Matrix modelling of harvesting effects in two contrasting habitats. *J. Appl. Ecol.* **45**, 41–51 (2008).

85. B. E. Kendall, *et al.*, Persistent problems in the construction of matrix population models. *Ecol. Model.* **406**, 33–43 (2019).

86. H. Caswell, Analysis of Life Table Response Experiments I. Decomposition of effects on population growth rate. *Ecol. Model.* **46**, 221–237 (1989).

87. S. P. Ellner, R. E. Snyder, P. B. Adler, G. Hooker, An expanded modern coexistence theory

for empirical applications. *Ecol. Lett.* **22**, 3–18 (2019).

88. G. Hooker, Generalized Functional ANOVA Diagnostics for High-Dimensional Functions of Dependent Variables. *J. Comput. Graph. Stat.* **16**, 709–732 (2007).

89. C. Hernandez, exactLTRE: An Exact Method for Life Table Response Experiment (LTRE) Analysis. (2022). Deposited 17 November 2022.

90. N. J. Enright, M. Franco, J. Silvertown, Comparing plant life histories using elasticity analysis: the importance of life span and the number of life-cycle stages. *Oecologia* **104**, 79–84 (1995).

91. O. R. Jones, *et al.*, Rcompadre and Rage - two R packages to facilitate the use of the COMPADRE and COMADRE databases and calculation of life history traits from matrix population models. *Methods Ecol. Evol.* **13**, 770–781 (2022).

92. R. Salguero-Gómez, J. B. Plotkin, Matrix dimensions bias demographic inferences: Implications for comparative plant demography. *Am. Nat.* **176**, 710–722 (2010).

93. M. E. Cochran, S. Ellner, Simple Methods for Calculating Age-Based Life History Parameters for Stage-Structured Populations. *Ecol. Monogr.* **62**, 345–364 (1992).

94. Demetrius, L., Entropy and the Life Table. *Naturwissenschaften* **65**, 435–436 (1978).

95. Capdevila, P., Walker, T. W. N., Schrodt, F., Rodriguez Caro, R. C., Salguero-Gomez, R., Global patterns of plant form and function are strongly determined by evolutionary relationships. *BioRxiv* (2023).

96. OpenTreeOfLife, *et al.*, Open Tree of Life Synthetic Tree. (2019).

97. L. J. Revell, phytools 2.0: an updated R ecosystem for phylogenetic comparative methods (and other things). *PeerJ* **12**, e16505 (2024).

98. E. Paradis, K. Schliep, ape 5.0: an environment for modern phylogenetics and evolutionary analyses in R. *Bioinformatics* **35** (2018).

99. A. Grafen, The phylogenetic regression. *Philos. Trans. R. Soc. Lond. B. Biol. Sci.* **326**, 119-157. (1989).

100. E. W. Goolsby, J. Bruggeman, C. Ané, Rphylopars: fast multivariate phylogenetic comparative methods for missing data and within-species variation. *Methods Ecol. Evol.* **8**, 22–27 (2017).

101. T. Merrien, K. Davis, M. D. Marco, P. Capdevila, R. Salguero-Gómez, Human pressures filter out the less resilient demographic strategies in natural populations of plants and animals worldwide. *BioRxiv* 1–36 (2022). https://doi.org/10.1101/2021.09.29.462372.

102. Orme, D., *et al.*, caper: Comparative Analyses of Phylogenetics and Evolution in R. (2023). Deposited 2023.

103. J. Kattge, *et al.*, TRY – a global database of plant traits. *Glob. Change Biol.* **17**, 2905–2935 (2011).

104. POWO, Plants of the World Online. Facilitated by the Royal Botanic Gardens, Kew. Published on the Internet. (2025). Available at: https://powo.science.kew.org/.

105. D. C. Adams, R. N. Felice, Assessing trait covariation and morphological integration on phylogenies using evolutionary covariance matrices. *PLoS ONE* **9** (2014).

106. G. Sanchez, plsdepot: Partial least squares (PLS) data analysis methods. (2012). Deposited 2012.

107. C. A. Bernaards, R. I. Jennrich, Gradient Projection Algorithms and Software for Arbitrary Rotation Criteria in Factor Analysis. *Educ. Psychol. Meas.* **65**, 676–696 (2005).

108. I. T. Jolliffe, J. Cadima, Principal component analysis: a review and recent developments. *Philos. Trans. R. Soc. Math. Phys. Eng. Sci.* **374**, 20150202 (2016).

109. C. P. Carmona, *et al.*, Fine-root traits in the global spectrum of plant form and function. *Nature* **597**, 683–687 (2021).

110. Bürkner, P., brms: An R Package for Bayesian Multilevel Models Using Stan. *J. Stat. Softw.* **80**, 1–28 (2017).

111. T. F. Wrycza, T. I. Missov, A. Baudisch, Quantifying the Shape of Aging. *PLOS ONE* **10**, e0119163 (2015).

936 **Figures & Tables**

937 **Figure 1**

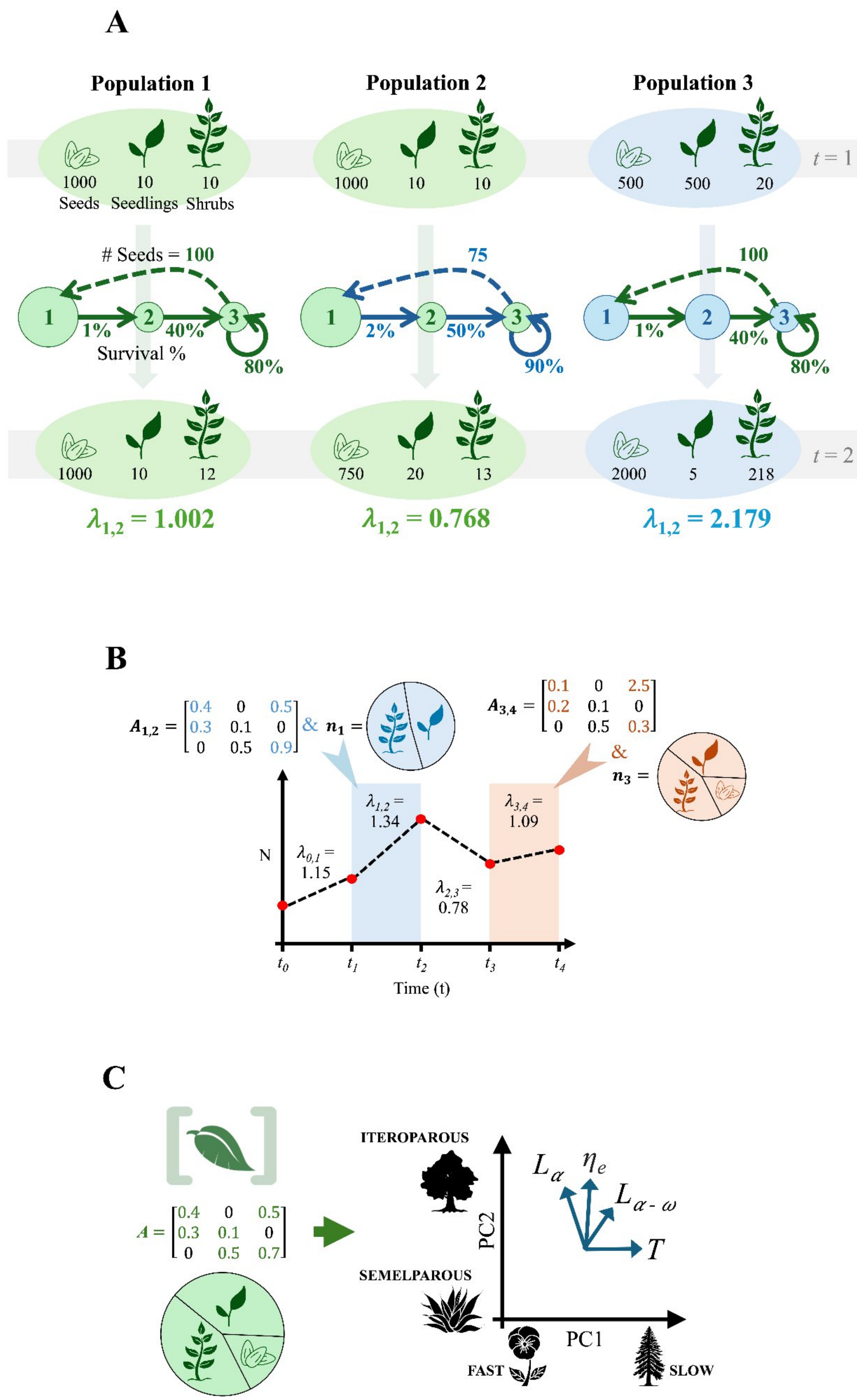

Figure 1. Our analytical pipeline to evaluate how the relative contributions of the vital rates and structure of a population to observed variation in demographic performance align with established life-history theory. (A) Variation across the realised growth rates expressed by natural populations are underpinned by changes in both their vital rates (*e.g.*, survival & fecundity) and structure (*i.e.*, the distribution of individuals across their life cycle). Consider three populations, each comprising the exact same population size (N_t = 1,020 individuals) at time t = 1. Two of these populations (Populations 1 & 2) have an identical structure but exhibit differing survival and fecundity rates, while two (Populations 1 & 3) have different structures but possess the same survival and fecundity rates. Despite these paired similarities, each population displays very different growth trajectories between times t = 1 and t = 2 owing to their differing structure and vital rate combinations, with Population 1 remaining stable ($\lambda_{1,2} \approx 1$), Population 2 declining ($\lambda_{1,2} < 1$), and Population 3 growing rapidly ($\lambda_{1,2} >> 1$). **(B)** Transient life table response experiments (tLTREs) decompose variation in short-term (*i.e.*, transient) population growth rates, observed across time, space, and experimental treatments, into the proportional contributions of changes in vital rates (***A***) and population structure (***n***). **(C)** We identified a sample of matrix population models (MPMs) describing temporal, spatial or experimental variation in the dynamics of different plant populations and corresponding census records describing their population structure from the COMPADRE database (22). Using these series of paired MPMs and population structures, we then evaluated how the proportional effects of vital rates and population structure on variance in $\lambda_{transient}$ corresponds with patterns across key life-history traits: generation time (T), age at reproductive maturity (L_α), mean life expectancy (η_e), and reproductive window ($L_{\alpha\text{-}\omega}$) (note the loadings shown are hypothetical representations).

960 **Figure 2**

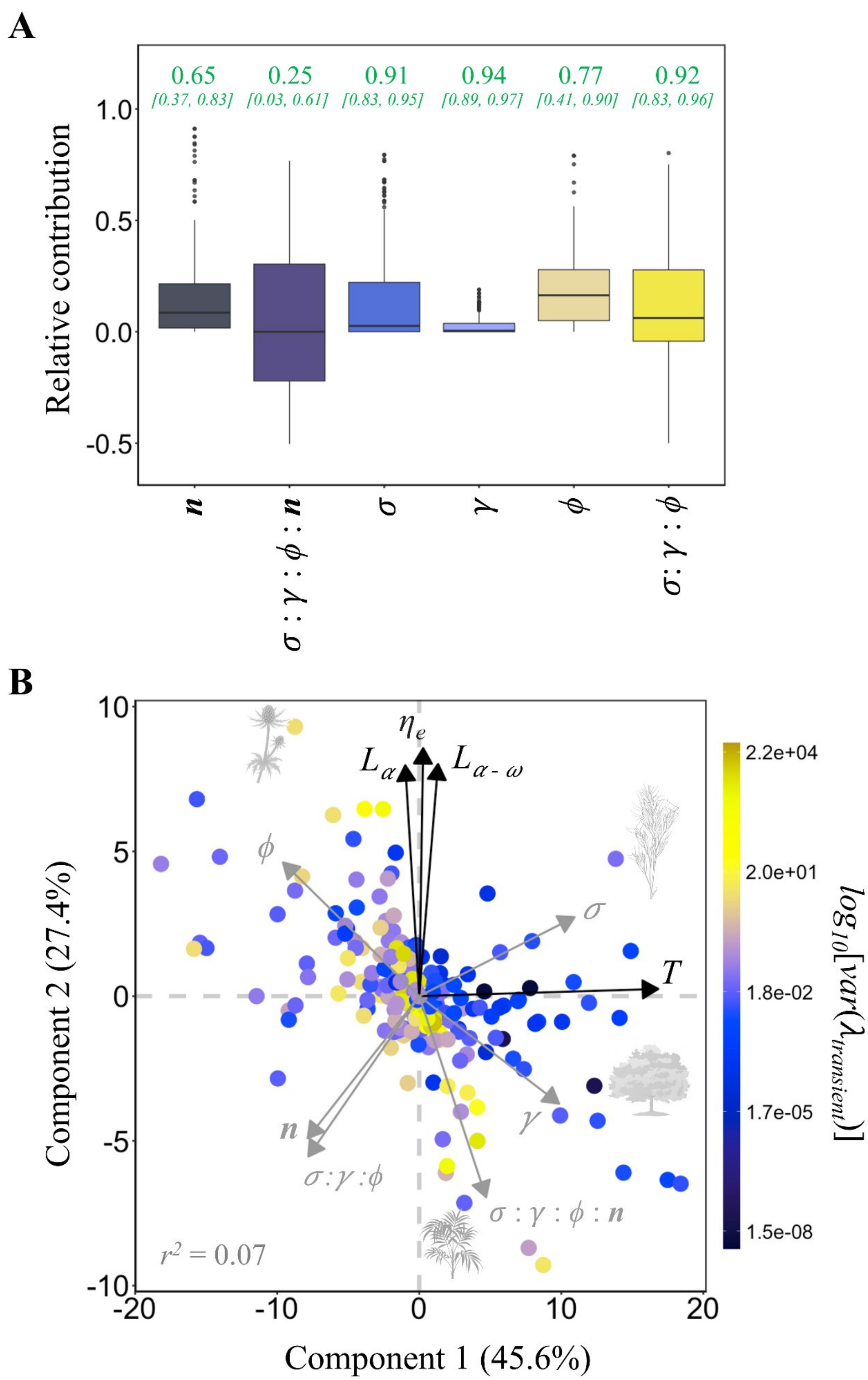
A
0.65
[0.37, 0.83]
0.25
[0.03, 0.61]
0.91
[0.83, 0.95]
0.94
[0.89, 0.97]
0.77
[0.41, 0.90]
0.92
[0.83, 0.96]
Relative contribution
1.0
0.5
0.0
-0.5
n
σ : γ : ϕ : n
σ
γ
ϕ
σ: γ : ϕ
B
Component 2 (27.4%)
Component 1 (45.6%)
10
5
0
-5
-10
-20
-10
0
10
20
η_e
L_α
L_α-ω
ϕ
σ
T
γ
n
σ:γ:ϕ
σ : γ : ϕ : n
r² = 0.07
2.2e+04
2.0e+01
1.8e-02
1.7e-05
1.5e-08
log10[var(λtransient)]

Figure 2. Variation in population structure has a comparable influence on observed variation in realised population growth rates ($\lambda_{transient}$) as fluctuations in survival and fecundity rates; particularly in species with faster life-history strategies. (A) The relative contributions observed across different sources of variance in $\lambda_{transient}$: Population structure ($\boldsymbol{n}$), the interactions between population structure and vital rates ($\sigma : \gamma : \phi : \boldsymbol{n}$), survival ($\sigma$), development ($\gamma$), fecundity ($\phi$), and the interactions between these vital rates ($\sigma : \gamma : \phi$). The inset values at the top illustrate the phylogenetic signal (Pagels Λ) associated with each contribution source, with error shown as 95% CIs. **(B)** Partial least squares biplot showing the relationship between sources of variation in $\lambda_{transient}$ and life-history traits: generation time (T), age at reproductive maturity (L_{α}), mean life expectancy (η_e), and reproductive window ($L_{\alpha\text{-}\omega}$). The colour scale depicts the log-transformed variance in $\lambda_{transient}$ recorded for population comparison. Representative species icons included adjacent to corresponding data point showing (top to bottom): *Eryngium alpinum* (Alpine sea holly), *Danthonia sericea* (Silky oat-grass), *Acer saccharum* (Sugar maple), and *Chamaedorea elegans* (Parlor palm).

Figure 3

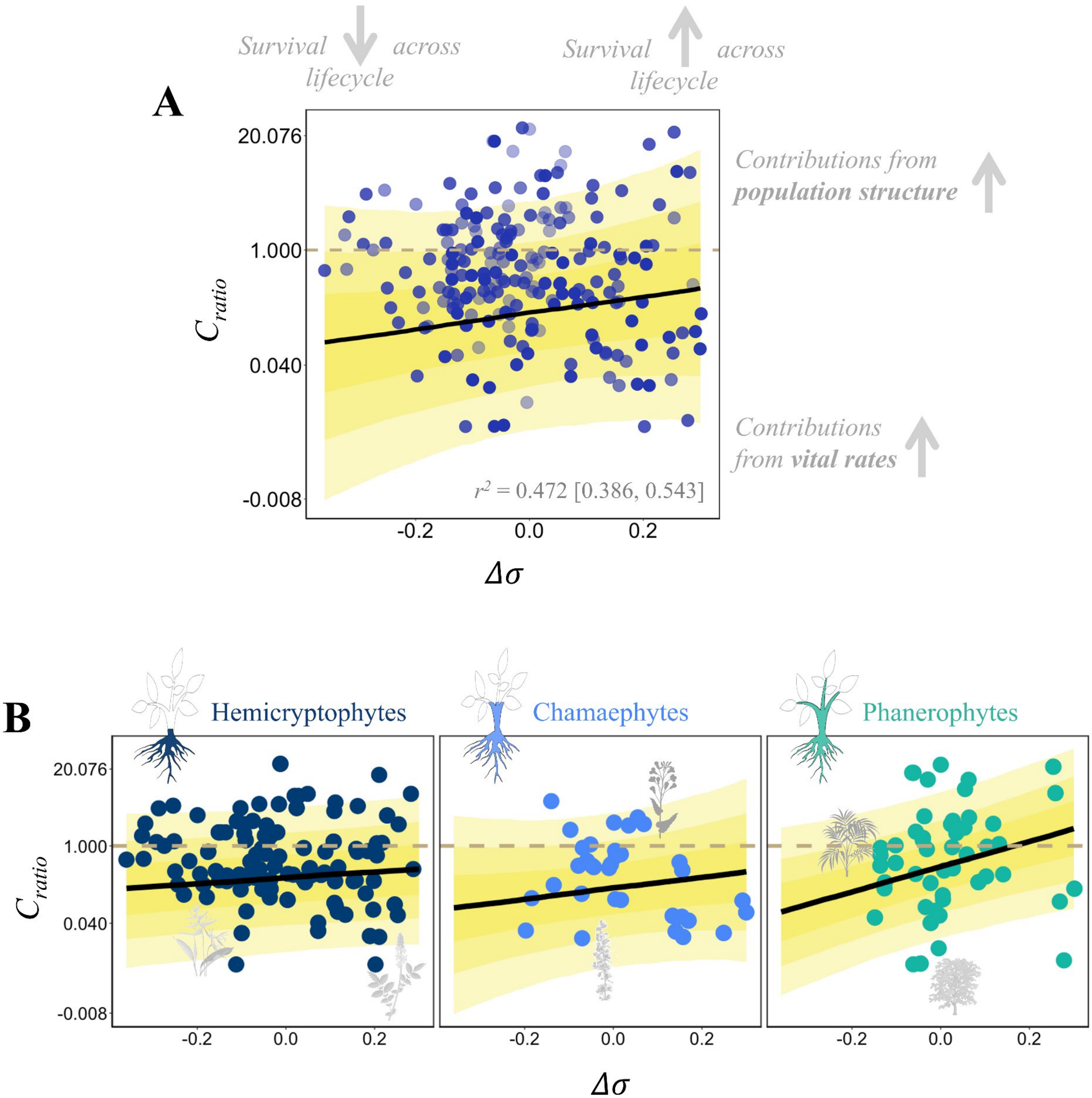

A
Survival across lifecycle
Survival across lifecycle
Contributions from **population structure**
Contributions from **vital rates**
r^2 = 0.472 [0.386, 0.543]
C_{ratio}
20.076
1.000
0.040
-0.008
-0.2
0.0
0.2
$\Delta\sigma$
B
Hemicryptophytes
Chamaephytes
Phanerophytes

Figure 3. Populations with life cycle survival profiles increasingly weighted towards survival in later life experience greater contributions from their population structure to variation in realised growth rates ($\lambda_{transient}$), a pattern that manifests consistently across plant growth strategies. (A) The relationship between $\Delta\sigma$ (*i.e.*, rate of change in stage-specific survival across the lifecycle) and contribution ratio estimates (C_{ratio}) across our 268 plant population comparisons. C_{ratio} estimates reflect the relative balance of contributions of population structure ($\boldsymbol{n}$) and vital rates ($\boldsymbol{A}$) toward observed variance in demographic performance, with the dashed line at C_{ratio} = 1 indicating equal contributions. Point shading differentiates between tLTRE assessments based on temporal, spatial, or experimental comparisons, or a combination of these cases (n: Time = 120, Space = 63, Experimental = 34, Combination = 51). Error displayed using 95% CIs. **(B)** The relationship between $\Delta\sigma$ and contribution ratio estimates (C_{ratio}) shown separately for Hemicrypophytes, Chamaephytes, and Phanerophytes. Error is displayed as 95% CI with the horizontal dashed line indicating the 1:1 threshold between contributions from vital rates and population structure. Representative species icons included adjacent to corresponding data point showing (left to right): *Heliconia acuminata* (Rich heliconia), *Agrimonia eupatoria* (Sticklewort), *Ambrosia dumosa* (White bursage), *Brassica insularis* (Indian mustard), *Chamaedorea elegans* (Parlor palm), and *Fagus grandifolia* (American beech).

Figure 4

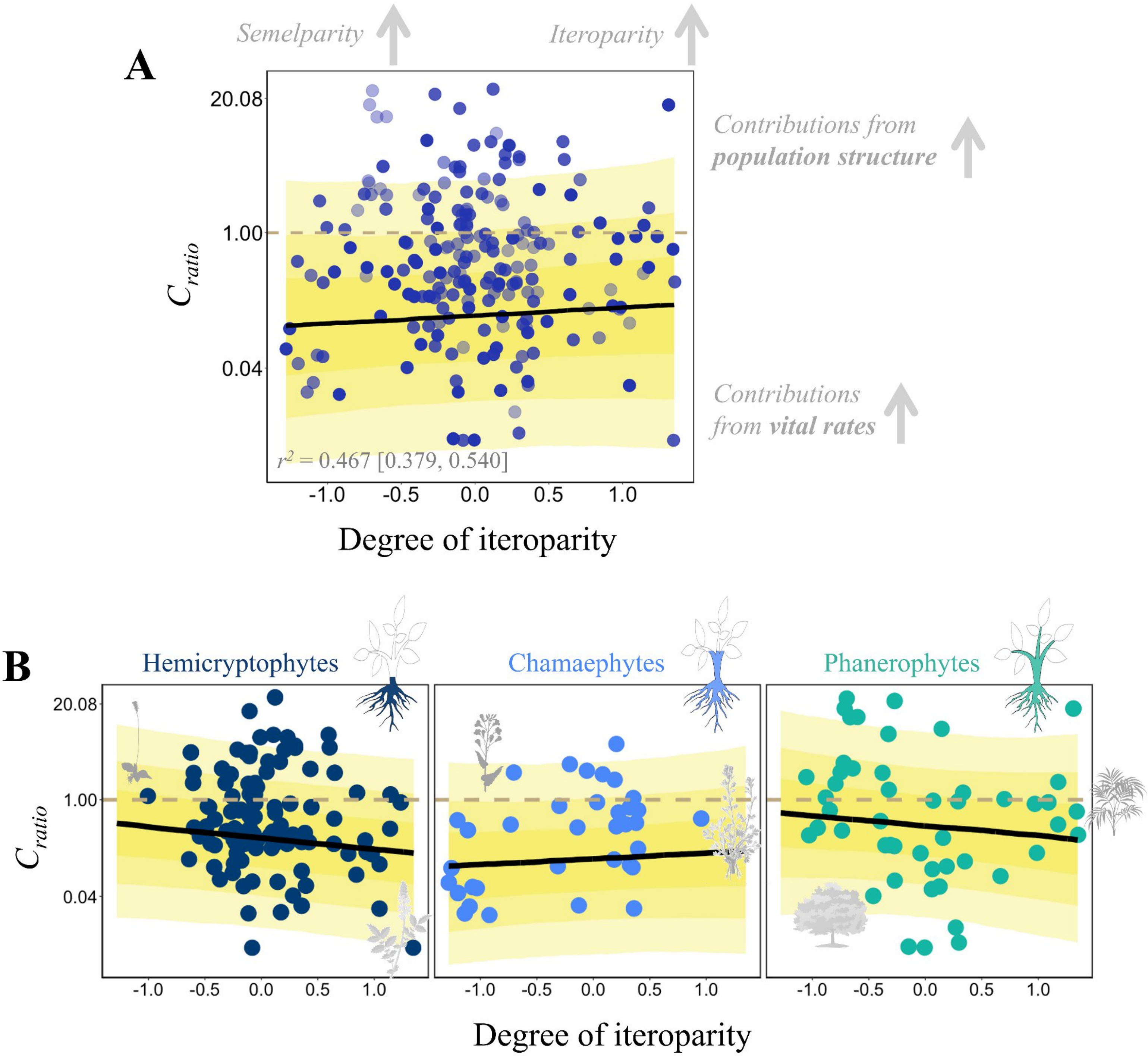
A
Semelparity
Iteroparity
Contributions from
population structure
Contributions
from vital rates
20.08
1.00
0.04
C ratio
r2 = 0.467 [0.379, 0.540]
-1.0
-0.5
0.0
0.5
1.0
Degree of iteroparity
B
Hemicryptophytes
Chamaephytes
Phanerophytes
Degree of iteroparity

Figure 4. The relationship between degree of iteroparity and the relative value of contributions from population structure to variation in realised growth rates ($\lambda_{transient}$) varies across plant growth forms. (A) The relationship between degree of iteroparity (*i.e.*, spread of reproduction through the life cycle) and contribution ratio estimates (C_{ratio}) across our 268 plant population comparisons. C_{ratio} estimates reflect the relative balance of contributions of population structure (***n***) and vital rates (***A***) toward observed variance in demographic performance, with the dashed line at C_{ratio} = 1 indicating equal contributions. Point shading differentiates between tLTRE assessments based on temporal, spatial, or experimental comparisons, or a combination of these cases (n: Time = 120, Space = 63, Experimental = 34, Combination = 51). Error displayed using 95% CIs. **(B)** The relationship between degree of iteroparity and contribution ratio estimates (C_{ratio}) shown separately for Hemicrypophytes, Chamaephytes, and Phanerophytes. Error is displayed as 95% CI with the horizontal dashed line indicating the 1:1 threshold between contributions from vital rates and population structure. Representative species icons included adjacent to corresponding data point showing (left to right): *Plantago media* (Hoary plantain), *Agrimonia eupatoria* (Sticklewort), *Brassica insularis* (Indian mustard), *Artemisia genipi* (Genipi), *Acer saccharum* (Sugar maple), and *Chamaedorea elegans* (Parlor palm).

Figure 5

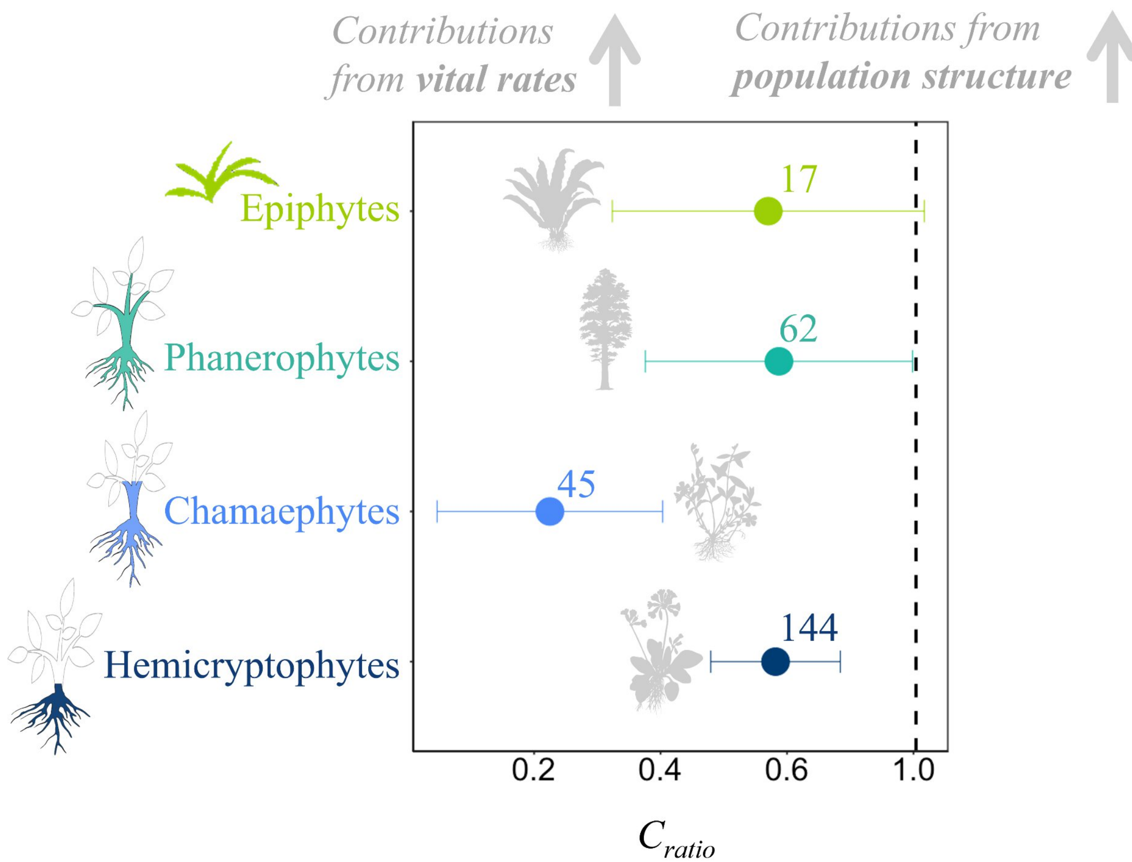

Figure 5. The relative importance of contributions of population structure *vs*. vital rates to variation in realised growth rates ($\lambda_{transient}$) varies across plant growth forms. Mean contribution ratio estimates (C_{ratio}) obtained for populations of plants classified as epiphytes (*e.g.*, Bird's nest Fern, *Asplenium nidus*), phanerophytes (*e.g.*, Giant sequoia, *Sequoiadendron giganteum*), chamaephytes (*e.g.*, Periwinkle, *Vinca minor*), and hemicryptophytes (*e.g.*, Cowslip, *Primula veris*). The vertical dashed line indicates equal contributions from vital rates and population structure to realised growth rates, while $C_{ratio} < 1$ implies a greater contribution from vital rates. Error bars display 95% CIs. Inset values indicate respective sample sizes obtained for each plant growth form.

Table 1. Definitions of the selected life-history traits used in this study.

Trait	Definition
Generation time (T)	Time steps required for individuals within a population to be replaced.
Mean life expectancy (η_e)	The average lifespan of individuals within a population.
Age at sexual maturity (L_α)	The average number of time steps taken by individuals to reach reproductive maturity.
Reproductive window ($L_{\alpha\text{-}\omega}$)	The average duration of reproduction in individuals across a population.
Life cycle survival profile ($\Delta\sigma$)	The rate of change in stage-specific survival across the lifecycle of a population. Higher values correspond with faster rates of change in stage-specific survival. Positive/negative values imply increases/decreases in survival throughout the lifecycle.
Mean lifetime survival ($\underline{\sigma}$)	Average survival probability of individuals across their lifecycle, irrespective of life-stage.
Degree of iteroparity (S)	Spread of reproduction through the lifespan of individuals. Higher/lower values correspond with greater iteroparity/semelparity.

Supporting Information for:

Life-history variation mediates the importance of population structure to the short-term dynamics of plant populations worldwide

James Cant, Christina M. Hernández, David N. Koons, Dave J. Hodgson, Man Qi, Andrew Hector, Iain Stott, Roberto Salguero-Gómez

Corresponding Authors: James Cant & Roberto Salguero-Gómez

Email: james.cant91@gmail.com; rob.salguero@biology.ox.ac.uk

This PDF file includes:

- Supporting text
- Figures S1 to S12
- Table S1
- SI References

Supporting Information Text:

S1. Evaluating the spatial representation of our tLTRE sample.

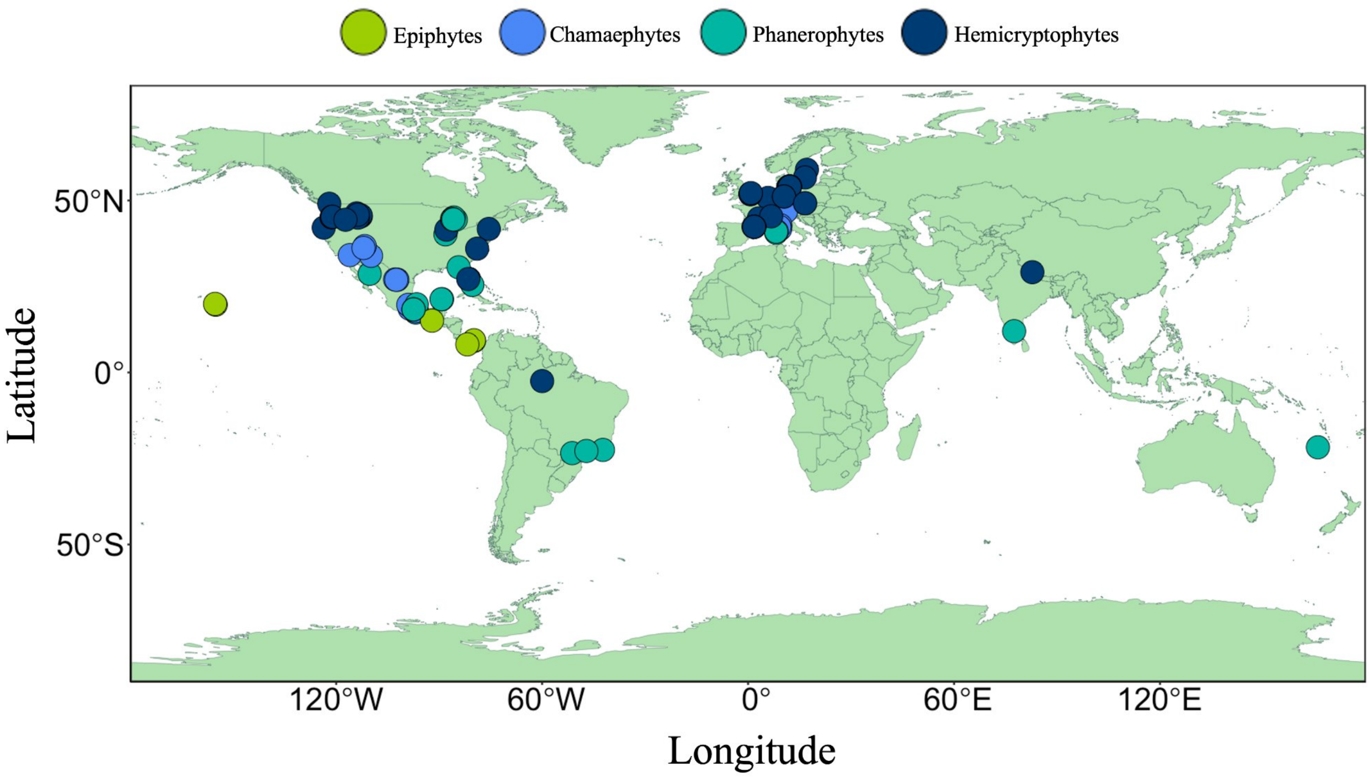

Figure S1. Recorded locations of all the unique populations represented by our 268 population comparisons across time, space, and experimental treatments. Points are coloured based on the Raunkiær growth form classification assigned to each population, with geophytes (n = 1) and hemicryptophytes (43) grouped as hemicryptophytes, and mega- (3), meso- (15), and nanophanerophytes (10) grouped as phanerophytes. Epiphytes and chamephytes are then represented by 6 and 16 populations, respectively.

S2. Excluding epiphytes from growth form comparisons.

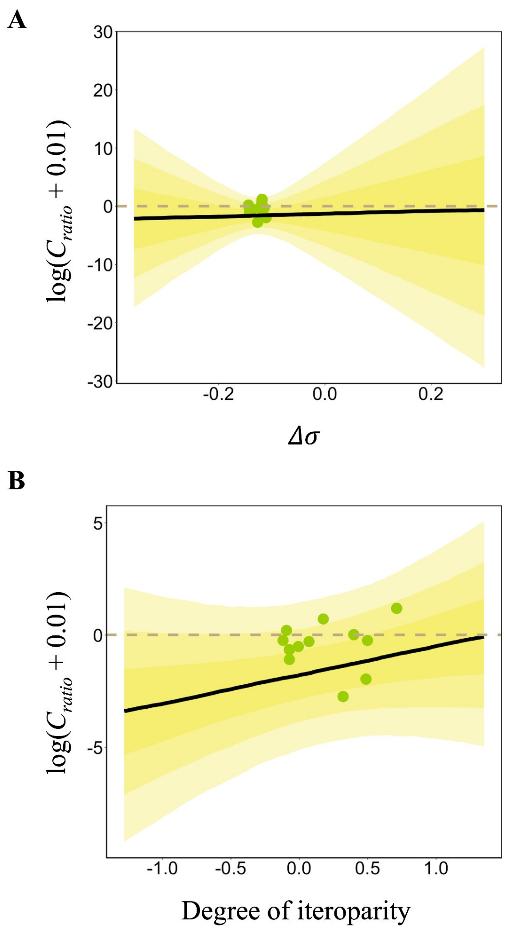

Figure S2. The epiphytic plant population comparisons included in our sample covered a limited range of life-cycle survival profile (*Δσ*) and degree of iteroparity (*S*) estimates, undermining the observed relationships between these life-history traits and contribution ratio estimates (C_{ratio}) reported for epiphytes. (A) The relationship between *Δσ* (*i.e.*, rate of change in stage-specific survival across the lifecycle) and contribution ratio estimates (C_{ratio}) obtained for 17 comparisons of epiphyte populations across time, space, and/or experimental treatments. **(B)** The relationship between degree of iteroparity and contribution ratio estimates (C_{ratio}) for the same 17 comparisons. C_{ratio} estimates reflect the relative balance of contributions of population structure (***n***) and vital rates (***A***) toward observed variance in demographic performance, with the dashed lines at C_{ratio} = 1 across both panels indicating equal contributions. Error displayed using 95% CIs.

S3. Quantifying life cycle survival profile ($\boldsymbol{\Delta\sigma}$).

As part of this study, we introduced the measure of life cycle survival profile ($\Delta\sigma$). Briefly, this measure describes the rate of change in stage-specific survival across the life cycle of a population. Higher absolute values of $|\Delta\sigma|$ correspond with more abrupt rates of change in stage-specific survival along the life cycle of the examined population, while positive/negative values imply increases/decreases in survival throughout its life cycle. Across our sample of 268 population comparisons, we estimated the element-by-element arithmetic mean matrix population model (MPM) from each associated set of MPMs describing the focal species/population dynamics across different time intervals, locations, or experimental treatments. We then collapsed each mean MPM into a 3 × 3 matrix, resulting in all comparisons comprising three life cycle stages to ensure comparability across populations and species. We carried out this step using the function *mpm_collapse* of the *Rcompadre* R package (1) to collapse together all life stages beyond the second life cycle stage into a single terminal stage while keeping the first two stages unaltered. This approach ensured we retained the eigen-structure of the original MPMs (2). We then computed $\Delta\sigma$ as the slope coefficient of a linear regression model fitted to the sequence of mean stage-specific survival probabilities obtained for each mean population/species MPM (*e.g.*, the slope of survival across life cycle stages). Below, we visually demonstrate the suitability of assuming that the gradient in stage-specific survival across three-stage life cycles can be appropriately modelled using a linear relationship. For this demonstration, we present the stage-specific survival (σ) patterns obtained for 30 randomly selected mean MPMs across our 268 population comparisons (Fig. S3), illustrating how, following the collapsing of each population's dynamics into a three-stage model, survival typically follows a linear rate of change across life stages.

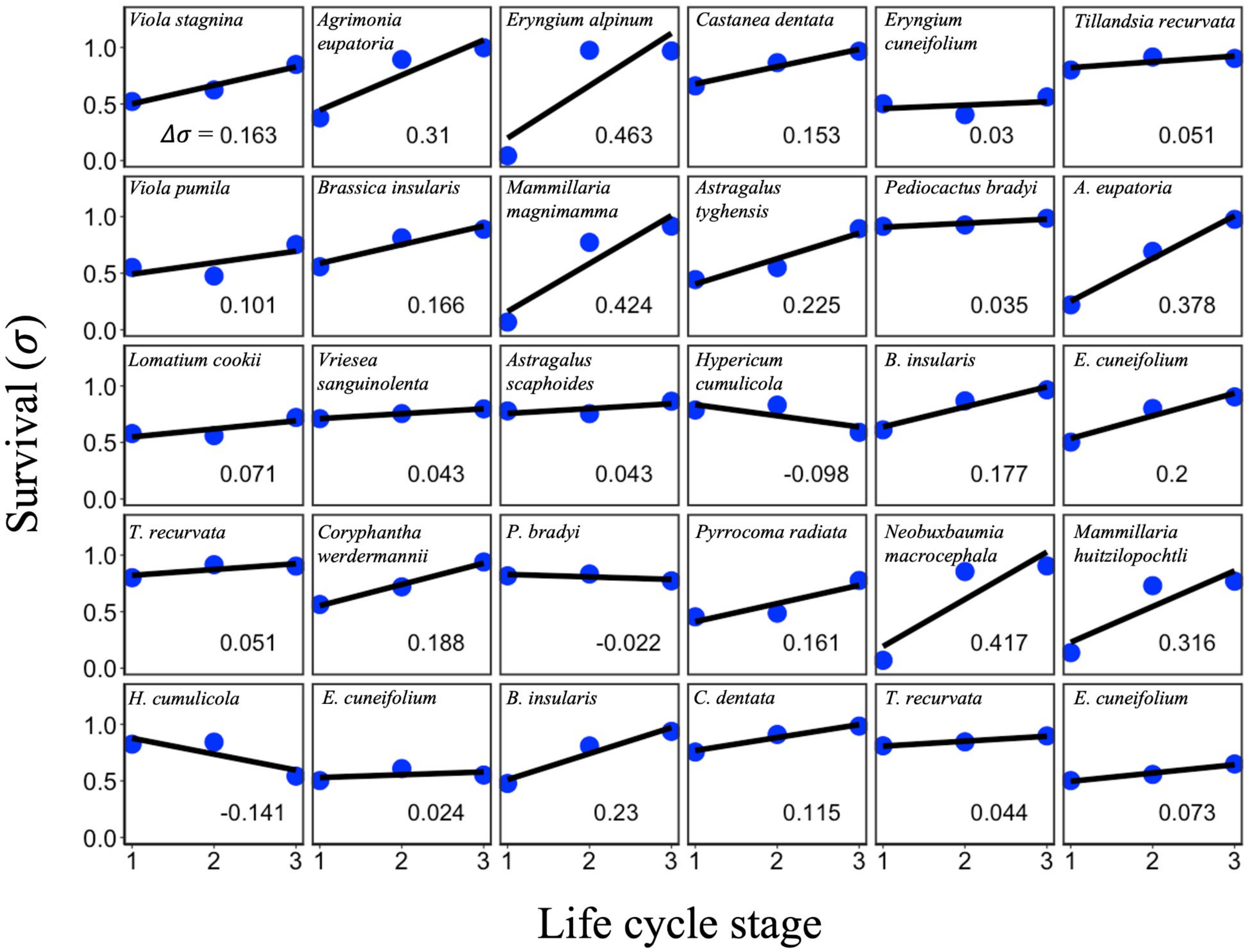

Figure S3. The mean stage-specific survival (*σ*) patterns across the life cycles of 30 plant populations randomly selected from our 268 population comparisons can be approximated via a linear model, whose slope is summarised by our metric: the life cycle survival profile (*Δσ*). Across each panel, the solid lines represent the linear relationship fit to each population's corresponding pattern in stage-specific survival (*σ*), with the inset text indicating the associated slope coefficient. Subsequently, these slope coefficients reflect the estimates of life cycle survival profile (*Δσ*) assigned to the selected populations.

S4. Testing sensitivity to pooling temporal, spatial, and experimental comparisons.

Our sample of 268 population comparisons comprises comparisons of population dynamics across time, space, and experimental treatments, or a combination of these cases (Time = 120 comparisons, Space = 63, Experimental = 34, Combination = 51). To test the sensitivity of our findings to our assumption that the short-term population growth rates in our plant dataset vary in the same fashion when comparisons are made across time, space, and experimental treatments, we repeated our analyses using only population comparisons across time. To do so, we repeated our analyses, implementing the same methodological pipeline as described in the main manuscript, but focused only on data sourced from population comparisons across time.

This brute-force sensitivity approach demonstrates how changes in population structure ($\boldsymbol{n}$) over time contribute to temporal variance in demographic performance to a similar extent as temporal shifts in survival (σ) and fecundity (ϕ) (Fig. S4A). Next, we reassessed the relationship between sources of variance in demographic performance and the life-history traits of generation time (T), age at reproductive maturity (L_{α}), mean life expectancy (η_e), and reproductive window ($L_{\alpha\text{-}\omega}$) (Fig. S4B). This analysis shows that the contributions from temporal shifts in survival to demographic performance correlate with generation time, while contributions from temporal shifts in population structure are greater in populations with shorter lifespans. We do note, however, that when only considering comparisons across time, the association between contributions from population structure to variance in demographic performance and shorter generation times becomes weaker (compare to Fig. 2).

Figure S4. The contribution of population structure to observed temporal variation in realised growth rates ($\lambda_{transient}$) is greater in species with faster life-history strategies. (A) The proportional effect distributions observed across different sources of temporal variance in $\lambda_{transient}$: Population structure (***n***), the interaction between population structure and vital rates ($\sigma : \gamma : \phi : \boldsymbol{n}$), survival ($\sigma$), development ($\gamma$), fecundity ($\phi$), and the interactions between these vital rates ($\sigma : \gamma : \phi$). **(B)** Partial least squares biplot showing the relationship between sources of temporal variation in $\lambda_{transient}$ and life-history traits: generation time (T), mean life expectancy (η_e), age at reproductive maturity (L_{α}), and reproductive window ($L_{\alpha\text{-}\omega}$). The

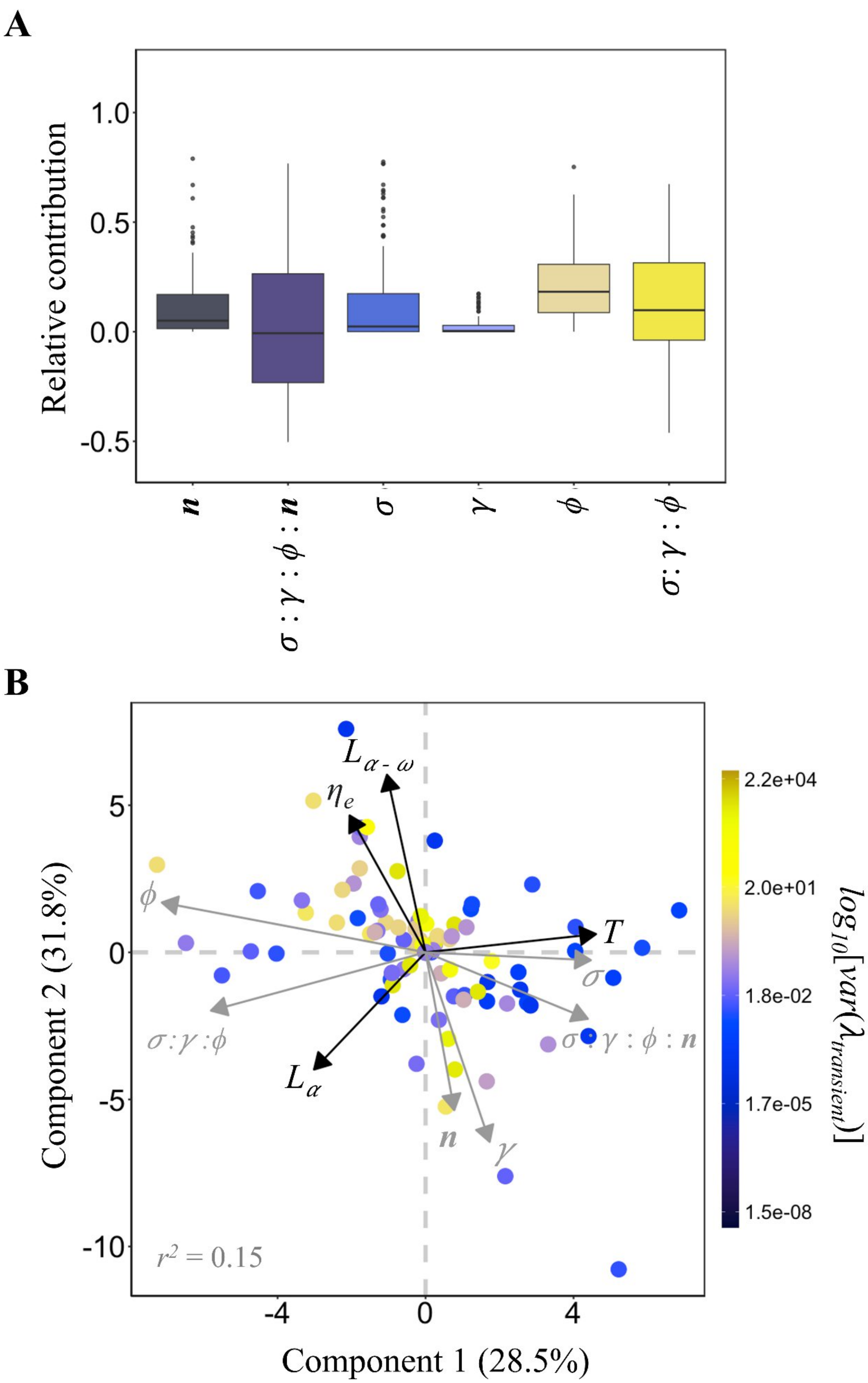

colour scale depicts the log-transformed variance in $\lambda_{transient}$ recorded for population comparison.

Pooling temporal, spatial, and experimental comparisons did have a slight influence on patterns between life-history traits and sources of variance in demographic performance across growth forms. Again, we computed estimates of contribution ratio (C_{ratio}) for each of our population comparisons, providing a measure of the balance between contributions from population structure *vs.* vital rates towards observed variance in demographic performance. Focusing only on temporal population comparisons, we observe how, although the relative patterns across C_{ratio} estimates obtained for hemicryptophytes, chamaephytes, and phanerophytes are maintained, the difference between estimates observed for chamaephytes and phanerophytes is diminished slightly (Fig. S5) compared to when spatial, temporal, and experimental comparisons are pooled (Fig. 5). We also observe how, when focusing on only temporal comparisons of population performance, C_{ratio} displays a negative relationship with the life cycle survival profile ($\Delta\sigma$) in both hemicryptophytes and chamaephytes (Fig. S6). This pattern is actually the reverse of the one obtained when temporal, spatial, and experimental comparisons are pooled (compare to Fig. 3). The pattern between $\Delta\sigma$ and C_{ratio} is, however, insensitive in phanerophytes across pooled and time-only comparisons. Finally, although stronger in time-only comparisons, the positive relationship observed between degree of iteroparity and C_{ratio} is maintained across pooled and time-only comparisons (Figs. S7, compared to Fig. 4). Thus, the primary findings we report are largely insensitive to our choice to pool temporal, spatial, and experimental comparisons of population dynamics in our analyses.

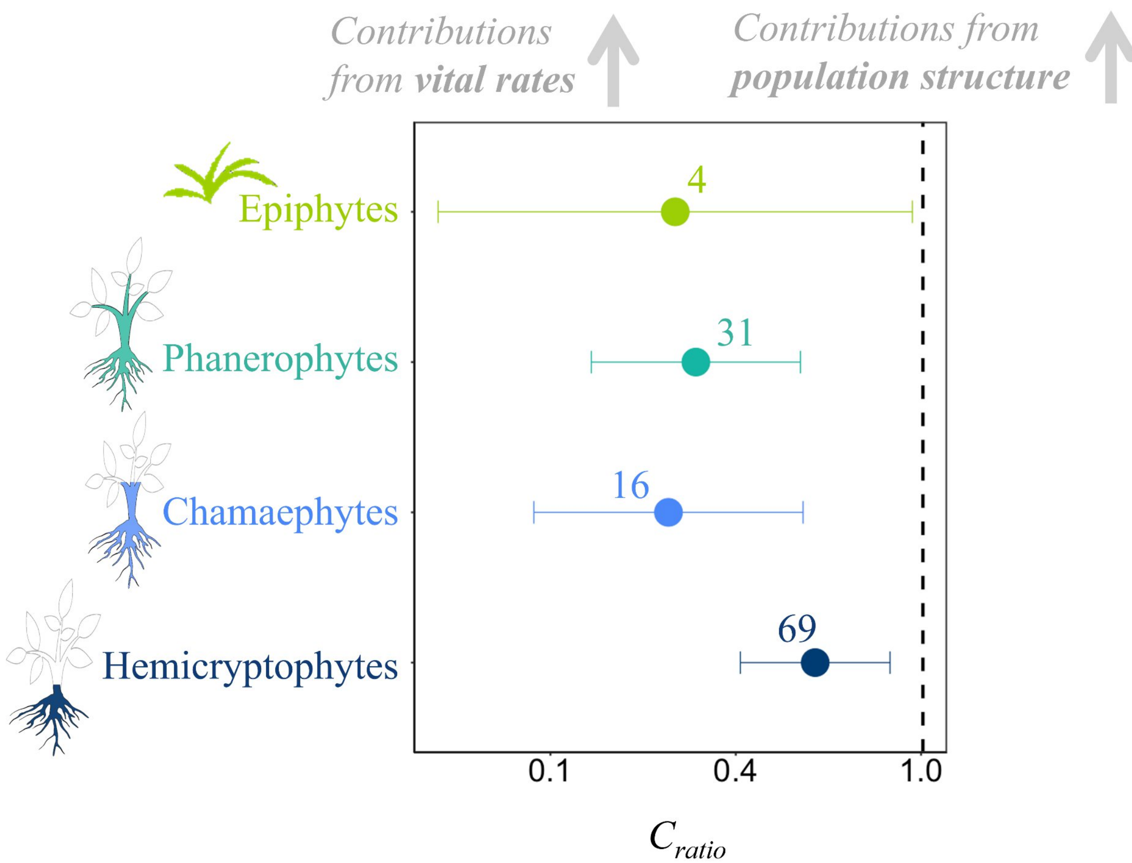

Figure S5. The relative importance of contributions of population structure *vs*. vital rates to observed temporal variation in realised growth rates ($\lambda_{transient}$) across plant growth forms. Mean contribution ratio estimates (C_{ratio}) obtained for populations of plants classified as epiphytes, phanerophytes, chamaephytes, and hemicryptophytes. The vertical dashed line indicates equal contributions from vital rates and population structure to realised growth rates, while $C_{ratio} < 1$ implies a greater contribution from vital rates. Error bars display 95% CIs. Inset values indicate respective sample sizes used for each plant growth form.

Figure S6. Populations with life cycle survival profiles increasingly weighted to survival in later life experience greater contributions from their population structure towards temporal variation in realised growth rates ($\lambda_{transient}$); a pattern that manifests consistently across plant growth strategies. **(A)** The relationship between $\Delta\sigma$ (*i.e.*, rate of change in stage-specific survival across the lifecycle) and contribution ratio estimates (C_{ratio}) across 120 comparisons of plant population dynamics through time. C_{ratio} estimates reflect the relative balance of contributions of population structure ($\boldsymbol{n}$) and vital rates ($\boldsymbol{A}$) toward observed variance in demographic performance, with the dashed line at C_{ratio} = 1 indicating equal contributions. Error displayed using 95% CIs. **(B)** The relationship between $\Delta\sigma$ and contribution ratio estimates (C_{ratio}) shown separately for Hemicrypophytes, Chamaephytes, and Phanerophytes. Error is displayed as 95% CI with the horizontal dashed line indicating the 1:1 threshold between contributions

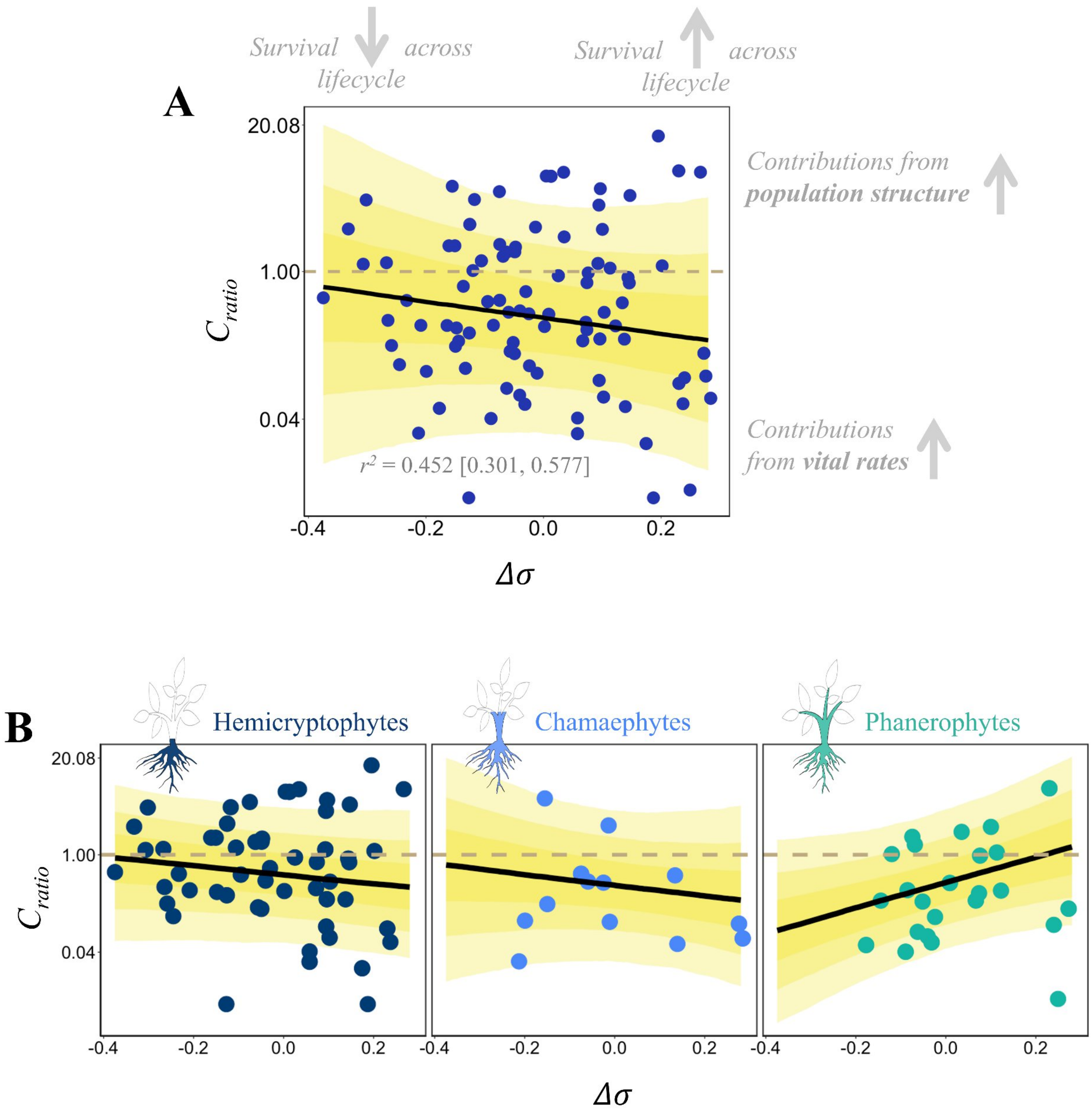

from vital rates and population structure.

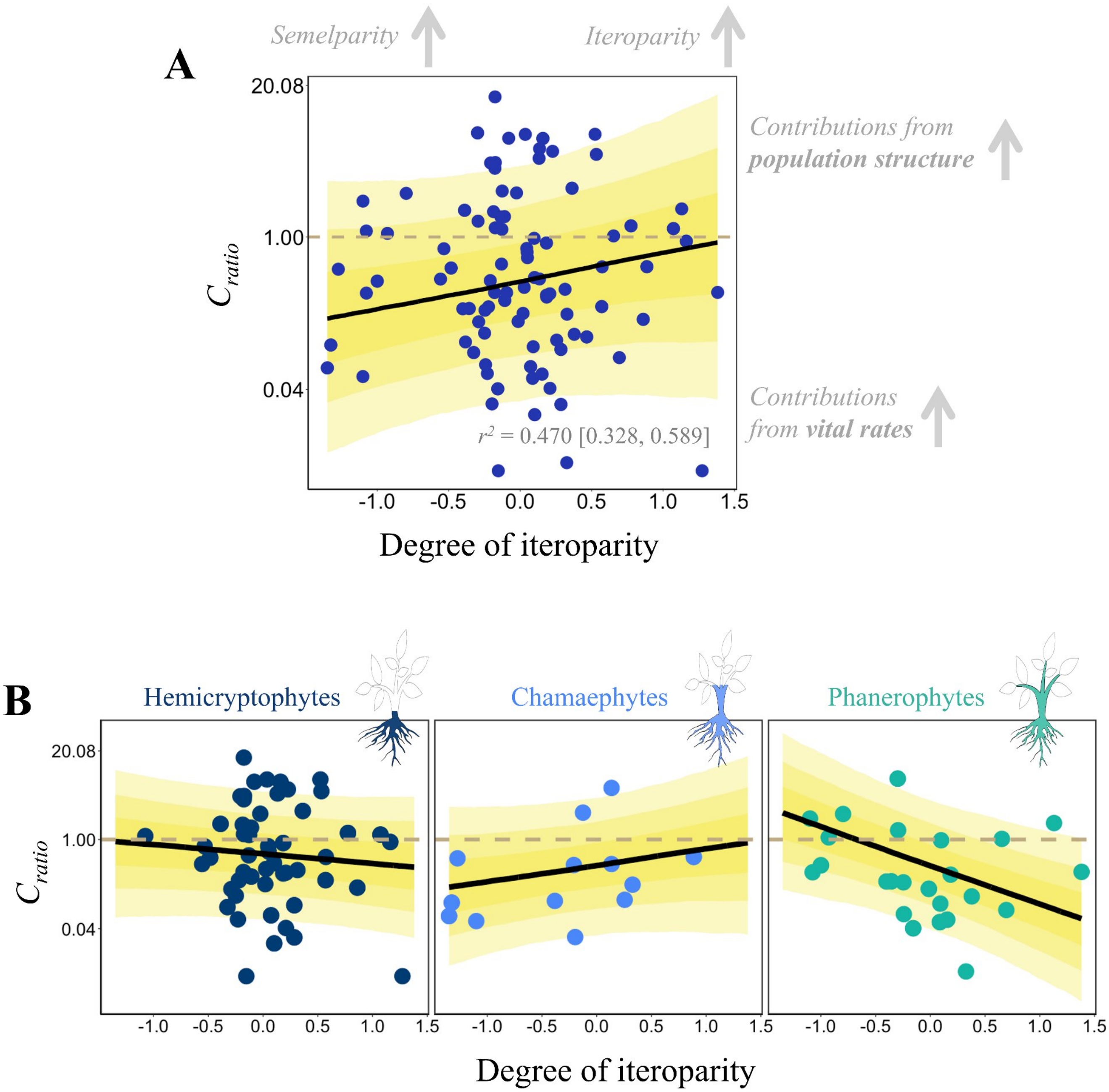

Figure S7. The relationship between degree of iteroparity and the relative value of contributions from population structure to temporal variation in realised growth rates ($\lambda_{transient}$) varies across plant growth forms. (A) The relationship between degree of iteroparity (*i.e.*, spread of reproduction through the life cycle) and contribution ratio estimates (C_{ratio}) across 120 comparisons of plant population dynamics through time. C_{ratio} estimates reflect the relative balance of contributions of population structure (***n***) and vital rates (***A***) toward observed variance in demographic performance, with the dashed line at C_{ratio} = 1 indicating equal contributions. Error displayed using 95% CIs. **(B)** The relationship between degree of iteroparity and contribution ratio estimates (C_{ratio}) is shown separately for Hemicrypophytes, Chamaephytes, and Phanerophytes. Error is displayed as 95% CI with the horizontal dashed line indicating the 1:1 threshold between contributions from vital rates and population structure.

S5. Testing sensitivity to data imputation.

During data extraction, we used phylogenetic imputations to estimate missing values across our demographic and life-history variables (Fig. S8). This step was necessary to allow us to retain details from all population comparisons within our finalised data sample, to limit the effect of data gaps on our demographic inferences (5). As such, we imputed estimates for one or more variables across 85 population comparisons. Combined, just 2.5% of our demographic and life-history trait data required imputing (Fig. S8). The majority of this missing data comprised estimates of the life-history traits: generation time (T), age at reproductive maturity (L_{α}), mean life expectancy (η_{e}), reproductive window ($L_{\alpha\text{-}\omega}$) and degree of iteroparity (S) (Fig. S8).

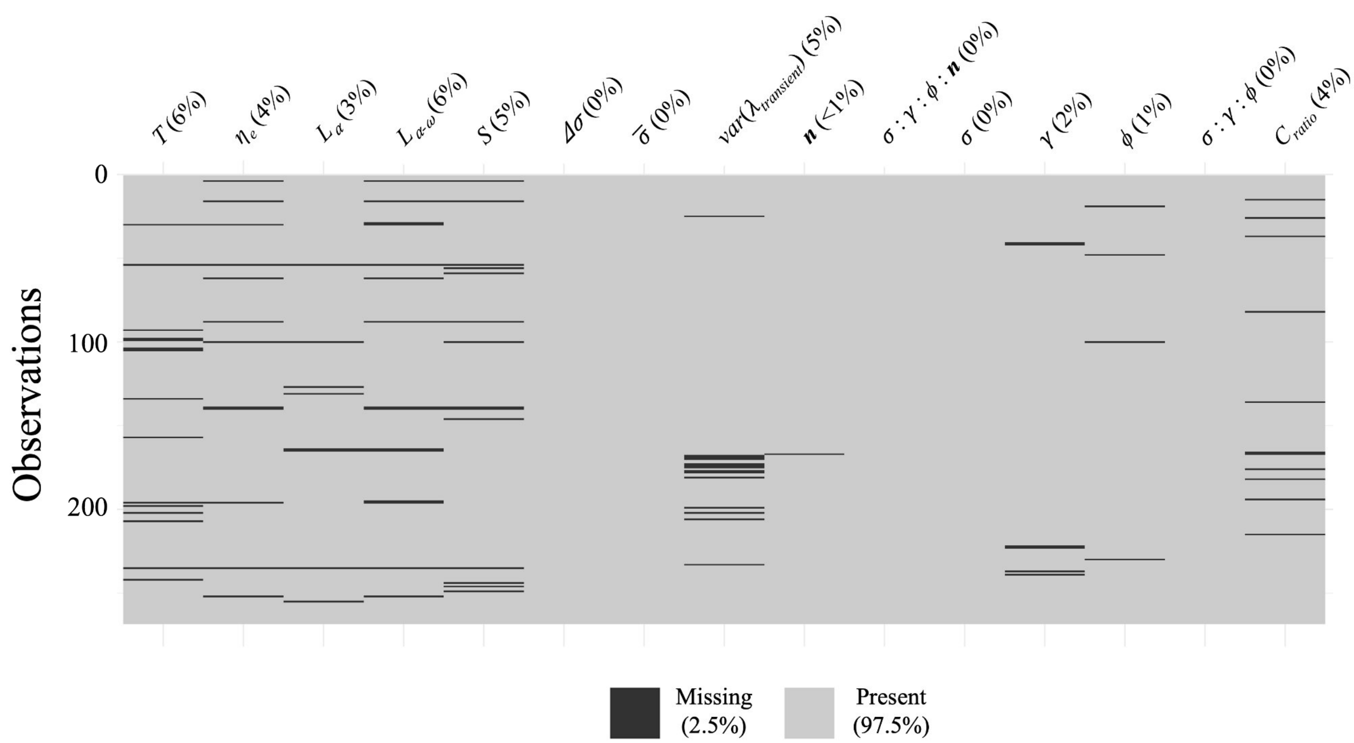

Figure S8. **Spread of missing data across our demographic and life-history trait variables.** Inset percentages indicate the degree of missing data across each variable.

To test the sensitivity of our findings to this imputation, we repeated the same methodological pipeline as described in the main manuscript, focusing on data sourced from population comparisons that required no imputation (183 population comparisons). Our brute-force sensitivity here also had no qualitative effect on our overall findings. First, contributions from changes in population structure (***n***) to observed variance in demographic performance remained comparable to those of changes in survival (σ) and fecundity (ϕ) (Fig. S9A). Second, contributions from changes in population structure (***n***) to observed variance in demographic performance were negatively correlated with generation time (*T*) (Fig. S9B). Instead, contributions from survival to demographic performance remained positively associated with generation time. Third, patterns in the relative balance between contributions from population structure *vs* vital rates towards observed variance in demographic performance (*i.e.*, contribution ratios, C_{ratio}) across hemicryptophytes, chamaephytes, and phanerophytes remained consistent between our non-imputed (Fig. S10) and full data samples (Fig. 5). Finally, the patterns we observed between life cycle survival profile ($\Delta\sigma$) and degree of iteroparity with C_{ratio} across growth forms remain consistent across our non-imputed (Fig. S11 & S12) and full data samples (Figs. 3 & 4).

Figure S9. The relationship between the contribution of population structure to observed variation in realised growth rates ($\lambda_{transient}$) and generation time remains intact even when focusing on the assessment of only non-imputed data. (A) The proportional effect distributions observed across different sources of temporal variance in $\lambda_{transient}$: Population structure ($\boldsymbol{n}$), the interaction between population structure and vital rates ($\sigma : \gamma : \phi : \boldsymbol{n}$), survival ($\sigma$), development ($\gamma$), fecundity ($\phi$), and the interactions between these vital rates ($\sigma : \gamma : \phi$). The inset values at the top illustrate the phylogenetic signal (Pagels λ) associated with each contribution source, with error shown as 95% CIs. **(B)** Partial least squares biplot showing the relationship between sources of temporal variation in $\lambda_{transient}$ and life-history traits: generation time (T), mean life expectancy (η_e), age at reproductive maturity (L_α), and reproductive window ($L_{\alpha\text{-}\omega}$). The

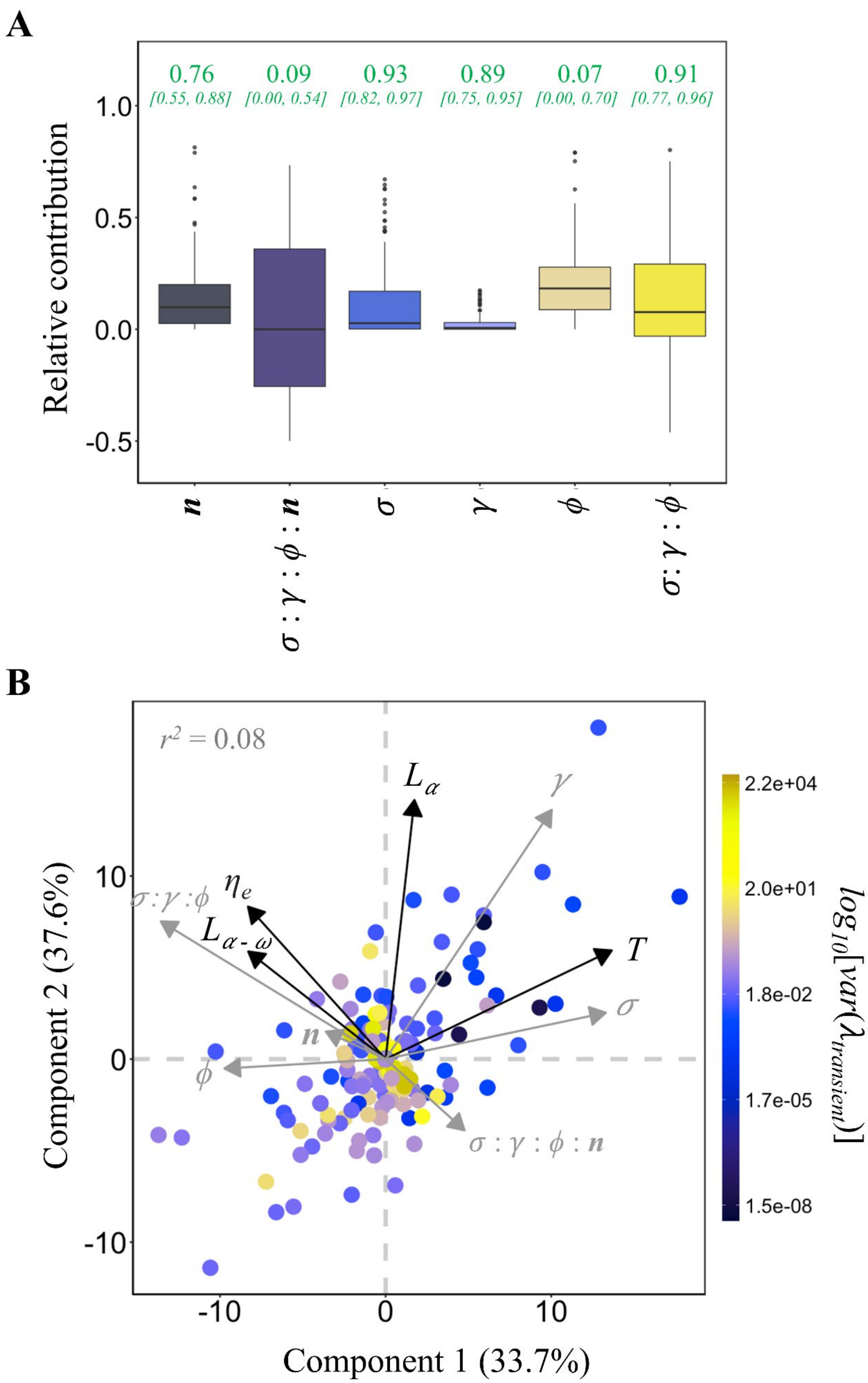

colour scale depicts the log-transformed variance in $\lambda_{transient}$ recorded for population comparison.

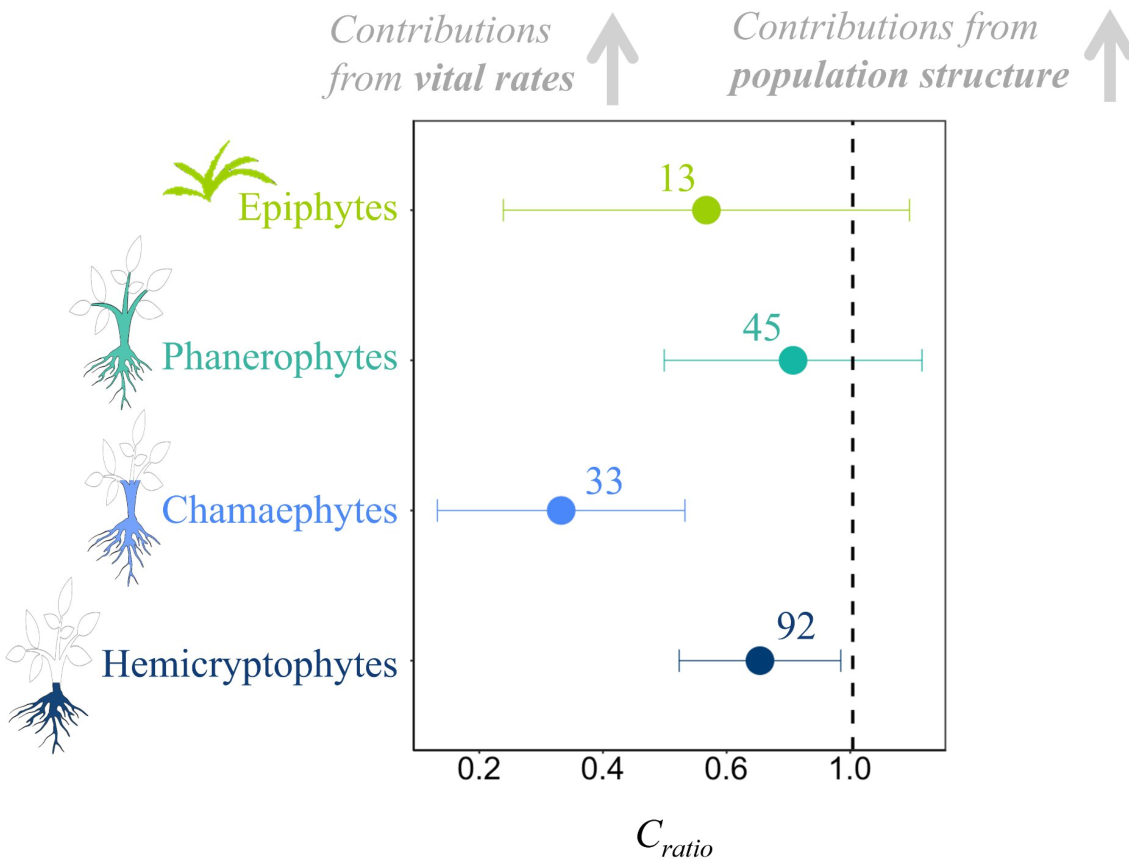

Figure S10. Variation in the relative importance of contributions of population structure *vs.* vital rates to temporal variation in realised growth rates ($\lambda_{transient}$) across plant growth forms is maintained when focusing on only non-imputed data. Mean contribution ratio estimates (C_{ratio}) obtained for populations of plants classified as epiphytes, phanerophytes, chamaephytes, and hemicryptophytes. The vertical dashed line indicates equal contributions from vital rates and population structure to realised growth rates, while $C_{ratio}< 1$ implies a greater contribution from vital rates. Error bars display 95% CIs. Inset values indicate respective sample sizes used for each plant growth form.

Figure S11. The relationships between life cycle survival profile (*Δσ*) and the relative contributions of population structure to variation in realised growth rates ($\lambda_{transient}$) across growth forms are maintained even when assessing only non-imputed data. (A) The relationship between *Δσ* (*i.e.*, rate of change in stage-specific survival across the lifecycle) and contribution ratio estimates (C_{ratio}) across 183 comparisons of plant population dynamics for which no data required imputing. C_{ratio} estimates reflect the relative balance of contributions of population structure (***n***) and vital rates (***A***) toward observed variance in demographic performance, with the dashed line at $C_{ratio} = 1$ indicating equal contributions. Error displayed using 95% CIs. **(B)** The relationship between *Δσ* and contribution ratio estimates (C_{ratio}) shown separately for Hemicrypophytes, Chamaephytes, and Phanerophytes. Error is displayed as 95% CI with the horizontal

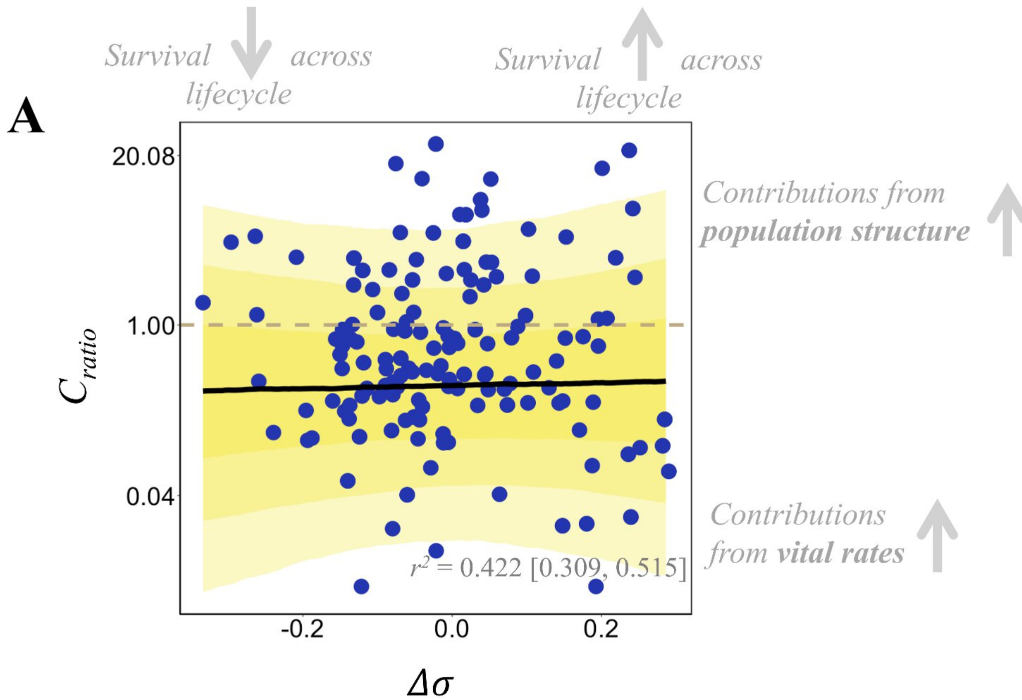

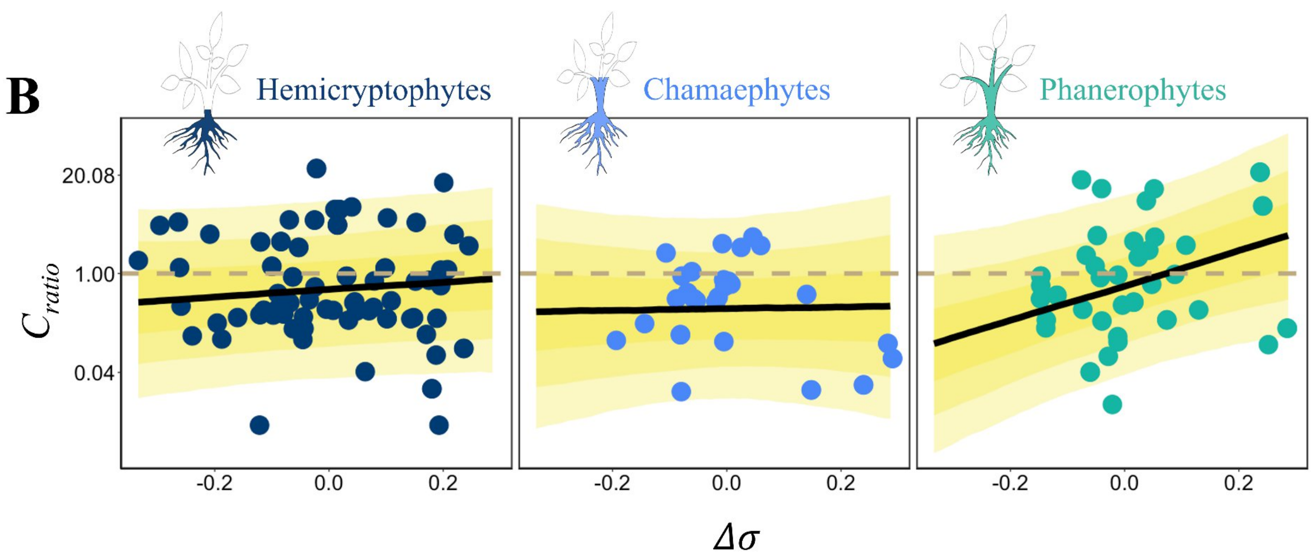

1241 dashed line indicating the 1:1 threshold between contributions from vital rates and population structure.

Figure S12. The relationships between degree of iteroparity and the relative contributions of population structure to variation in realised growth rates ($\lambda_{transient}$) across growth forms are maintained even when assessing only non-imputed data. (A) The relationship between degree of iteroparity (*i.e.*, spread of reproduction through the life cycle) and contribution ratio estimates (C_{ratio}) across 183 comparisons of plant population dynamics for which no data required imputing. C_{ratio} estimates reflect the relative balance of contributions of population structure (***n***) and vital rates (***A***) toward observed variance in demographic performance, with the dashed line at C_{ratio} = 1 indicating equal contributions. Error displayed using 95% CIs. **(B)** The relationship between degree of iteroparity and contribution ratio estimates (C_{ratio}) shown separately for Hemicrypophytes, Chamaephytes, and Phanerophytes. Error is displayed as 95% CI with the horizontal dashed line indicating the 1:1 threshold between contributions

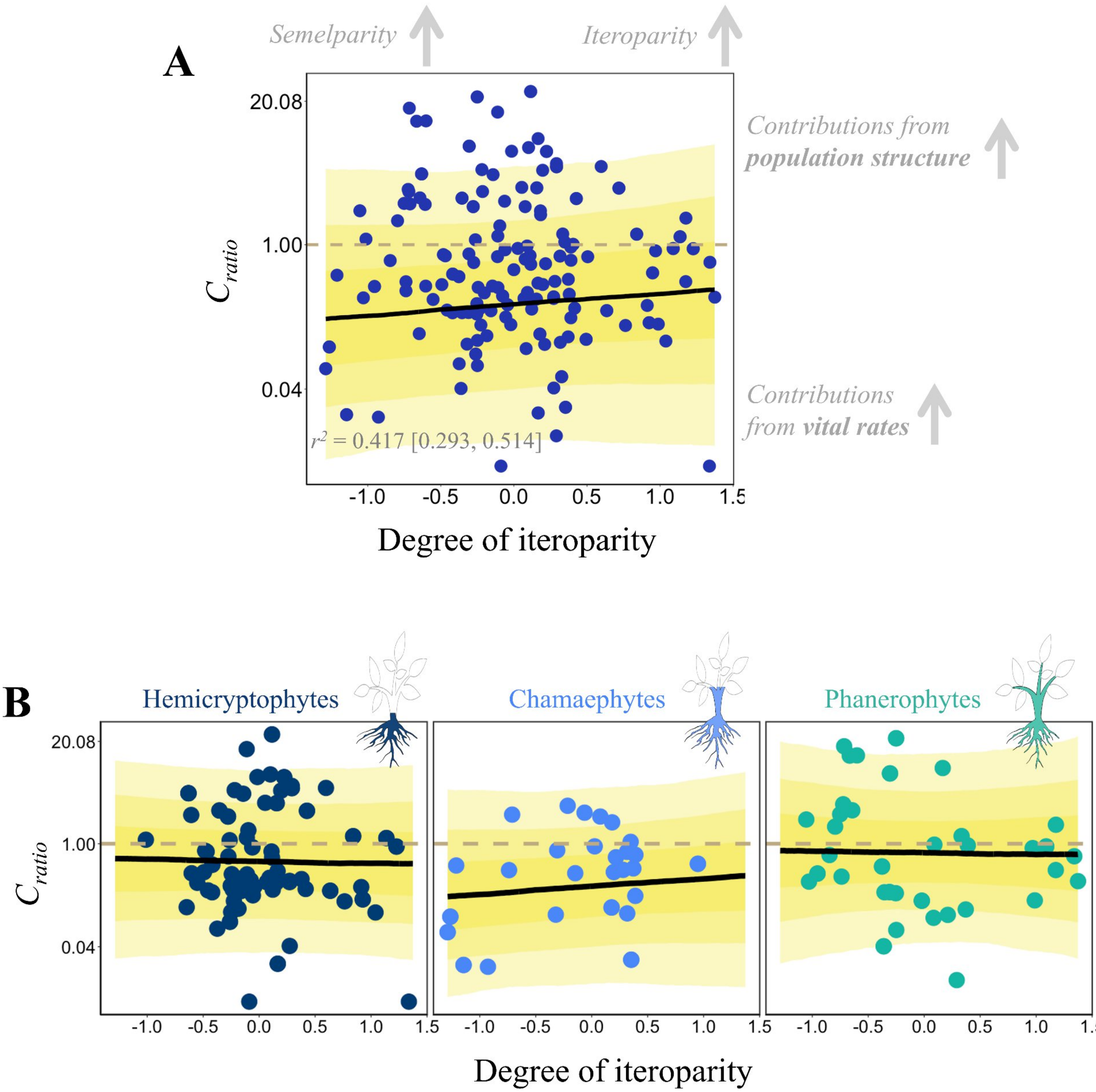

from vital rates and population structure.

Table S1. A summary of the 268 population comparisons used in this study. This table shows the number of matrix population models (MPMs) included for each comparison (# MPM), the number of life cycle stages represented by each model (# stages), whether the sets of MPMs describe comparisons across time, space, or experimental treatments, or combinations of these cases (LTRE comparison), and the Raunkiær growth form classification (6) assigned to the plant species associated with each comparison.

Species	# MPM	# stages	LTRE comparison	Raunkiær growth form
Acer saccharum	2	3	Time	Megaphanerophyte
Actaea elata	2	6	Time	Hemicryptophyte
Actinostemon concolor	2	3	Time	Nanophanerophyte
Agrimonia eupatoria	2	4	Space	Hemicryptophyte
Agrimonia eupatoria	2	4	Space	Hemicryptophyte
Artemisia genipi	2	5	Treatment	Chamaephyte
Artemisia genipi	2	5	Time	Chamaephyte
Attalea humilis	2	5	Treatment	Nanophanerophyte
Boswellia papyrifera	2	12	Treatment	Mesophanerophyte
Bursera glabrifolia	2	5	Time	Nanophanerophyte
Chamaedorea elegans	2	6	Treatment	Nanophanerophyte
Chamaedorea elegans	2	6	Treatment	Nanophanerophyte
Chamaedorea elegans	2	6	Treatment	Nanophanerophyte
Chamaedorea elegans	2	6	Time	Nanophanerophyte
Chamaedorea elegans	2	6	Time	Nanophanerophyte
Clidemia hirta	2	5	Space	Epiphyte

Coryphantha werdermannii	2	6	Multiple	Chamaephyte
Coryphantha werdermannii	2	6	Multiple	Chamaephyte
Coryphantha werdermannii	2	6	Multiple	Chamaephyte
Danthonia sericea	2	6	Time	Hemicryptophyte
Danthonia sericea	2	6	Time	Hemicryptophyte
Danthonia sericea	2	6	Time	Hemicryptophyte
Dicerandra frutescens	2	6	Treatment	Nanophanerophyte
Eryngium cuneifolium	2	6	Space	Hemicryptophyte
Eryngium cuneifolium	2	6	Multiple	Hemicryptophyte
Eryngium cuneifolium	2	6	Space	Hemicryptophyte
Eryngium cuneifolium	2	6	Multiple	Hemicryptophyte
Fagus grandifolia	2	9	Treatment	Megaphanerophyte
Heliconia acuminata	2	6	Treatment	Geophyte
Heliconia acuminata	2	6	Treatment	Geophyte
Liatris scariosa	2	5	Multiple	Hemicryptophyte
Liatris scariosa	2	5	Multiple	Hemicryptophyte
Liatris scariosa	2	5	Multiple	Hemicryptophyte
Liatris scariosa	2	5	Multiple	Hemicryptophyte
Liatris scariosa	2	5	Time	Hemicryptophyte
Lomatium cookii	2	6	Space	Hemicryptophyte
Lomatium cookii	2	6	Space	Hemicryptophyte
Lomatium cookii	2	6	Space	Hemicryptophyte

Lomatium cookii	2	6	Space	Hemicryptophyte
Mammillaria crucigera	2	8	Time	Chamaephyte
Mammillaria huitzilopochtli	2	5	Multiple	Chamaephyte
Mammillaria huitzilopochtli	2	5	Multiple	Chamaephyte
Mammillaria huitzilopochtli	2	5	Multiple	Chamaephyte
Mammillaria huitzilopochtli	2	5	Multiple	Chamaephyte
Mammillaria huitzilopochtli	2	5	Multiple	Chamaephyte
Mammillaria magnimamma	2	7	Multiple	Chamaephyte
Mammillaria magnimamma	2	7	Time	Chamaephyte
Manilkara zapota	2	9	Time	Mesophanerophyte
Nardostachys jatamansi	2	6	Treatment	Hemicryptophyte
Nardostachys jatamansi	2	6	Treatment	Hemicryptophyte
Nardostachys jatamansi	2	6	Treatment	Hemicryptophyte
Nardostachys jatamansi	2	6	Treatment	Hemicryptophyte
Neobuxbaumia tetetzo	2	10	Time	Mesophanerophyte
Pachycereus pecten-aboriginum	2	9	Time	Mesophanerophyte
Primula veris	2	6	Time	Hemicryptophyte
Primula vulgaris	2	5	Time	Hemicryptophyte
Primula vulgaris	2	5	Time	Hemicryptophyte
Primula vulgaris	2	5	Time	Hemicryptophyte
Primula vulgaris	2	5	Time	Hemicryptophyte

Primula vulgaris	2	5	Time	Hemicryptophyte
Primula vulgaris	2	5	Time	Hemicryptophyte
Pseudophoenix sargentii	2	5	Treatment	Mesophanerophyte
Pterocereus gaumeri	2	10	Space	Mesophanerophyte
Pterocereus gaumeri	2	10	Time	Mesophanerophyte
Sanicula europaea	2	5	Treatment	Hemicryptophyte
Sanicula europaea	2	5	Treatment	Hemicryptophyte
Sanicula europaea	2	5	Treatment	Hemicryptophyte
Sanicula europaea	2	5	Treatment	Hemicryptophyte
Sanicula europaea	2	5	Treatment	Hemicryptophyte
Sanicula europaea	2	5	Treatment	Hemicryptophyte
Tillandsia recurvata	2	4	Multiple	Epiphyte
Tillandsia recurvata	2	4	Multiple	Epiphyte
Tillandsia recurvata	2	4	Multiple	Epiphyte
Tillandsia recurvata	2	4	Time	Epiphyte
Trollius europaeus	2	6	Space	Hemicryptophyte
Trollius europaeus	2	6	Time	Hemicryptophyte
Viola elatior	2	5	Space	Hemicryptophyte
Viola pumila	2	5	Space	Hemicryptophyte
Viola stagnina	2	5	Space	Hemicryptophyte
Vriesea sanguinolenta	2	7	Space	Epiphyte
Vriesea sanguinolenta	2	7	Space	Epiphyte

Vriesea sanguinolenta	2	7	Space	Epiphyte
Acer saccharum	2	3	Time	Megaphanerophyte
Acer saccharum	3	3	Space	Megaphanerophyte
Actaea elata	2	6	Time	Hemicryptophyte
Actinostemon concolor	2	3	Time	Nanophanerophyte
Agrimonia eupatoria	2	4	Time	Hemicryptophyte
Agrimonia eupatoria	2	4	Space	Hemicryptophyte
Agrimonia eupatoria	2	4	Space	Hemicryptophyte
Agrimonia eupatoria	4	4	Time	Hemicryptophyte
Ambrosia dumosa	4	6	Treatment	Chamaephyte
Ambrosia dumosa	4	6	Treatment	Chamaephyte
Boechera fecunda	3	4	Space	Hemicryptophyte
Boechera fecunda	3	4	Space	Hemicryptophyte
Boechera fecunda	3	4	Space	Hemicryptophyte
Boechera fecunda	3	4	Space	Hemicryptophyte
Boechera fecunda	6	4	Time	Hemicryptophyte
Boechera fecunda	4	4	Time	Hemicryptophyte
Boechera fecunda	4	4	Time	Hemicryptophyte
Araucaria laubenfelsii	3	4	Treatment	Megaphanerophyte
Artemisia genipi	2	5	Treatment	Chamaephyte
Artemisia genipi	2	5	Time	Chamaephyte
Astragalus scaphoides	10	5	Time	Hemicryptophyte

Astragalus scaphoides	9	5	Time	Hemicryptophyte
Astragalus scaphoides	8	5	Time	Hemicryptophyte
Astragalus tyghensis	6	5	Time	Hemicryptophyte
Astragalus tyghensis	6	5	Time	Hemicryptophyte
Astragalus tyghensis	7	5	Time	Hemicryptophyte
Astragalus tyghensis	5	5	Time	Hemicryptophyte
Astragalus tyghensis	6	5	Time	Hemicryptophyte
Attalea humilis	2	5	Treatment	Nanophanerophyte
Boswellia papyrifera	2	12	Treatment	Mesophanerophyte
Brassica insularis	3	3	Space	Chamaephyte
Brassica insularis	4	3	Space	Chamaephyte
Brassica insularis	4	3	Space	Chamaephyte
Brassica insularis	3	3	Space	Chamaephyte
Brassica insularis	4	3	Space	Chamaephyte
Brassica insularis	4	3	Space	Chamaephyte
Brassica insularis	3	3	Space	Chamaephyte
Brassica insularis	3	3	Space	Chamaephyte
Brassica insularis	3	3	Space	Chamaephyte
Brassica insularis	8	3	Time	Chamaephyte
Brassica insularis	5	3	Time	Chamaephyte
Brassica insularis	9	3	Time	Chamaephyte
Brassica insularis	9	3	Time	Chamaephyte

Bursera glabrifolia	2	5	Time	Nanophanerophyte
Castanea dentata	6	8	Multiple	Mesophanerophyte
Castanea dentata	6	8	Multiple	Mesophanerophyte
Castanea dentata	6	8	Multiple	Mesophanerophyte
Castanea dentata	5	8	Multiple	Mesophanerophyte
Castanea dentata	4	8	Time	Mesophanerophyte
Castanea dentata	4	8	Time	Mesophanerophyte
Castanea dentata	4	8	Time	Mesophanerophyte
Castanea dentata	3	8	Time	Mesophanerophyte
Castanea dentata	4	8	Time	Mesophanerophyte
Castanea dentata	4	8	Time	Mesophanerophyte
Centaurea horrida	3	5	Space	Nanophanerophyte
Chamaedorea elegans	3	6	Treatment	Nanophanerophyte
Clidemia hirta	2	5	Space	Epiphyte
Clidemia hirta	2	5	Time	Epiphyte
Coryphantha werdermannii	3	6	Multiple	Chamaephyte
Danthonia sericea	2	6	Time	Hemicryptophyte
Danthonia sericea	2	6	Time	Hemicryptophyte
Danthonia sericea	2	6	Time	Hemicryptophyte
Danthonia sericea	3	6	Space	Hemicryptophyte
Danthonia sericea	5	6	Space	Hemicryptophyte
Dicerandra frutescens	2	6	Multiple	Nanophanerophyte

Dicerandra frutescens	3	6	Multiple	Nanophanerophyte
Dicerandra frutescens	3	6	Multiple	Nanophanerophyte
Dicerandra frutescens	3	6	Multiple	Nanophanerophyte
Dicerandra frutescens	3	6	Multiple	Nanophanerophyte
Dicerandra frutescens	2	6	Multiple	Nanophanerophyte
Dicerandra frutescens	3	6	Multiple	Nanophanerophyte
Dicerandra frutescens	2	6	Multiple	Nanophanerophyte
Dicerandra frutescens	2	6	Multiple	Nanophanerophyte
Dicerandra frutescens	5	6	Time	Nanophanerophyte
Dicerandra frutescens	3	6	Time	Nanophanerophyte
Dicerandra frutescens	3	6	Time	Nanophanerophyte
Dicerandra frutescens	5	6	Time	Nanophanerophyte
Dicerandra frutescens	11	6	Time	Nanophanerophyte
Eriogonum longifolium	4	5	Time	Hemicryptophyte
Eriogonum longifolium	4	5	Time	Hemicryptophyte
Eriogonum longifolium	8	5	Time	Hemicryptophyte
Eryngium alpinum	2	4	Multiple	Hemicryptophyte
Eryngium alpinum	3	4	Time	Hemicryptophyte
Eryngium cuneifolium	4	6	Time	Hemicryptophyte
Eryngium cuneifolium	3	6	Time	Hemicryptophyte
Eryngium cuneifolium	7	6	Time	Hemicryptophyte
Eryngium cuneifolium	8	6	Time	Hemicryptophyte

Eryngium cuneifolium	7	6	Time	Hemicryptophyte
Eryngium cuneifolium	2	6	Multiple	Hemicryptophyte
Eryngium cuneifolium	2	6	Space	Hemicryptophyte
Eryngium cuneifolium	5	6	Multiple	Hemicryptophyte
Eryngium cuneifolium	3	6	Space	Hemicryptophyte
Eryngium cuneifolium	5	6	Multiple	Hemicryptophyte
Eryngium cuneifolium	3	6	Space	Hemicryptophyte
Eryngium cuneifolium	4	6	Multiple	Hemicryptophyte
Eryngium cuneifolium	3	6	Space	Hemicryptophyte
Eryngium cuneifolium	4	6	Multiple	Hemicryptophyte
Eryngium cuneifolium	3	6	Space	Hemicryptophyte
Eryngium cuneifolium	2	6	Multiple	Hemicryptophyte
Eryngium cuneifolium	2	6	Space	Hemicryptophyte
Eryngium cuneifolium	2	6	Multiple	Hemicryptophyte
Euterpe edulis	3	7	Time	Mesophanerophyte
Fagus grandifolia	2	9	Treatment	Megaphanerophyte
Guarianthe aurantiaca	2	5	Time	Epiphyte
Pyrrocoma radiata	7	4	Time	Hemicryptophyte
Pyrrocoma radiata	7	4	Time	Hemicryptophyte
Pyrrocoma radiata	7	4	Time	Hemicryptophyte
Pyrrocoma radiata	6	4	Time	Hemicryptophyte
Pyrrocoma radiata	6	4	Time	Hemicryptophyte

Pyrrocoma radiata	6	4	Time	Hemicryptophyte
Pyrrocoma radiata	5	4	Time	Hemicryptophyte
Pyrrocoma radiata	5	4	Time	Hemicryptophyte
Heliconia acuminata	2	6	Treatment	Geophyte
Heliconia acuminata	2	6	Treatment	Geophyte
Hypericum cumulicola	4	6	Space	Hemicryptophyte
Hypericum cumulicola	4	6	Space	Hemicryptophyte
Hypericum cumulicola	3	6	Space	Hemicryptophyte
Hypericum cumulicola	3	6	Space	Hemicryptophyte
Hypericum cumulicola	4	6	Space	Hemicryptophyte
Hypericum cumulicola	4	6	Time	Hemicryptophyte
Hypericum cumulicola	3	6	Time	Hemicryptophyte
Hypericum cumulicola	3	6	Time	Hemicryptophyte
Hypericum cumulicola	4	6	Time	Hemicryptophyte
Hypericum cumulicola	4	6	Time	Hemicryptophyte
Hypericum cumulicola	4	6	Time	Hemicryptophyte
Liatris scariosa	2	5	Multiple	Hemicryptophyte
Liatris scariosa	3	5	Multiple	Hemicryptophyte
Liatris scariosa	3	5	Time	Hemicryptophyte
Liatris scariosa	2	5	Time	Hemicryptophyte
Lomatium cookii	4	6	Time	Hemicryptophyte
Lomatium cookii	4	6	Time	Hemicryptophyte

Lomatium cookii	2	6	Space	Hemicryptophyte
Lomatium cookii	2	6	Space	Hemicryptophyte
Lomatium cookii	2	6	Space	Hemicryptophyte
Lomatium cookii	2	6	Space	Hemicryptophyte
Lomatium cookii	4	6	Time	Hemicryptophyte
Lomatium cookii	4	6	Time	Hemicryptophyte
Mammillaria crucigera	2	8	Time	Chamaephyte
Mammillaria huitzilopochtli	5	5	Time	Chamaephyte
Mammillaria huitzilopochtli	2	5	Multiple	Chamaephyte
Mammillaria huitzilopochtli	2	5	Multiple	Chamaephyte
Mammillaria huitzilopochtli	2	5	Multiple	Chamaephyte
Mammillaria huitzilopochtli	2	5	Multiple	Chamaephyte
Mammillaria huitzilopochtli	2	5	Multiple	Chamaephyte
Mammillaria huitzilopochtli	5	5	Time	Chamaephyte
Mammillaria magnimamma	2	7	Multiple	Chamaephyte
Mammillaria magnimamma	2	7	Time	Chamaephyte
Manilkara zapota	2	9	Time	Mesophanerophyte
Nardostachys jatamansi	5	6	Treatment	Hemicryptophyte
Neobuxbaumia macrocephala	3	10	Time	Mesophanerophyte
Neobuxbaumia mezcalaensis	3	10	Time	Mesophanerophyte
Neobuxbaumia tetetzo	2	10	Time	Mesophanerophyte

Pachycereus pecten-aboriginum	2	9	Time	Mesophanerophyte
Pediocactus bradyi	4	3	Time	Chamaephyte
Pediocactus bradyi	5	3	Time	Chamaephyte
Pediocactus bradyi	4	3	Time	Chamaephyte
Pediocactus bradyi	13	3	Time	Chamaephyte
Phyllanthus indofischeri	5	7	Time	Mesophanerophyte
Plantago media	3	5	Time	Hemicryptophyte
Plantago media	2	5	Time	Hemicryptophyte
Primula veris	2	6	Time	Hemicryptophyte
Primula vulgaris	7	5	Space	Hemicryptophyte
Primula vulgaris	7	5	Space	Hemicryptophyte
Primula vulgaris	2	5	Time	Hemicryptophyte
Primula vulgaris	2	5	Time	Hemicryptophyte
Primula vulgaris	2	5	Time	Hemicryptophyte
Primula vulgaris	2	5	Time	Hemicryptophyte
Primula vulgaris	2	5	Time	Hemicryptophyte
Primula vulgaris	2	5	Time	Hemicryptophyte
Pseudophoenix sargentii	2	5	Treatment	Mesophanerophyte
Pterocereus gaumeri	2	10	Space	Mesophanerophyte
Pterocereus gaumeri	2	10	Time	Mesophanerophyte
Ramonda myconi	2	5	Space	Hemicryptophyte

Sanicula europaea	4	5	Treatment	Hemicryptophyte
Tillandsia recurvata	2	4	Multiple	Epiphyte
Tillandsia recurvata	2	4	Multiple	Epiphyte
Tillandsia recurvata	2	4	Multiple	Epiphyte
Tillandsia recurvata	6	4	Space	Epiphyte
Tillandsia recurvata	2	4	Time	Epiphyte
Trollius europaeus	3	6	Space	Hemicryptophyte
Trollius europaeus	2	6	Space	Hemicryptophyte
Trollius europaeus	2	6	Time	Hemicryptophyte
Viola elatior	2	5	Space	Hemicryptophyte
Viola pumila	2	5	Space	Hemicryptophyte
Viola stagnina	2	5	Space	Hemicryptophyte
Vriesea sanguinolenta	3	7	Space	Epiphyte

Supporting Information References

1. O. R. Jones, *et al.*, Rcompadre and Rage - two R packages to facilitate the use of the COMPADRE and COMADRE databases and calculation of life history traits from matrix population models. *Methods Ecol. Evol.* **13**, 770–781 (2022).

2. R. Salguero-Gómez, J. B. Plotkin, Matrix dimensions bias demographic inferences: Implications for comparative plant demography. *Am. Nat.* **176**, 710–722 (2010).

3. R. Salguero-Gómez, *et al.*, Fast–slow continuum and reproductive strategies structure plant life-history variation worldwide. *Proc. Natl. Acad. Sci.* **113**, 220–235 (2016).

4. P. Capdevila, *et al.*, Life history mediates the trade-offs among different components of demographic resilience. *Ecol. Lett.* **00**, 1–14 (2022).

5. T. D. James, R. Salguero-Gómez, O. R. Jones, D. Z. Childs, A. P. Beckerman, Bridging gaps in demographic analysis with phylogenetic imputation. *Conserv. Biol.* **35**, 1210–1221 (2021).

6. C. Raunkiaer, *The life forms of plants and statistical plant geography; being the collected papers of C. Raunkiaer.* (1934).